	Fe
18	Cr
10	Ni
+	Ti

Type 321

1 GENERAL

Type 321 is an austenitic stainless steel, which can be hardened by cold work but not by heat treatment. Its composition is similar to that of Type 304, except that titanium is added to form stable precipitates of titanium carbide randomly distributed within the grains. In the stabilization heat-treated condition, harmful precipitation of chromium carbides at the grain boundaries in the sensitization range of 800 to 1600 F is prevented and the alloy has good resistance to intergranular corrosion. Type 321 and other stabilized grades of stainless steels such as Types 347 and 348 are preferred for long-time service in the 800 to 1600 F range, while Type 304L is frequently employed for applications involving welding or short-time heating in this temperature range. Although they are both equally insensitive to grain-boundary carbide precipitation and intergranular corrosion, Type 321 is somewhat inferior to Type 347 in general corrosion resistance. Since the titanium in Type 321 is readily oxidized during melting, it is rarely employed for welding rods or for castings. Some of the more important applications for this alloy are in aircraft collector rings and exhaust manifolds, expansion joints, high-temperature chemical processing equipment, and pressure vessels (8,9,11,33).

1.01 Commercial Designation

Type 321.

1.02 Alternate Designations

Type 321H (11), UNS S32100, UNS S32109-(321H), UNS J92630.

1.03 Specifications

1.031 Table 1.031.

1.04 Composition

1.041 Table 1.041.

1.05 Heat Treatment

1.051 Anneal: 1750 F to 2050 F, air cool or water quench. This treatment results in maximum ductility and workability and minimum hardness (8,9,33). Highly reducing annealing atmospheres should be avoided (11).

1.052 Stabilization: 1550 to 1650 F 2 hours, air cool or water quench. This treatment, following the annealing treatment, is recommended for the most severe conditions of service, particularly those above 800 F. (See also 1.091.) The purpose is to reprecipitate, as titanium carbide, carbon dissolved during the anneal, and thereby to reduce the tendency to form chromium carbides during service. Generally, the higher the annealing temperature, the greater the need for a stabilizing heat treatment (8,33).

1.053 Process anneal or stress relief: 1300 F, air cool. This treatment or, alternatively, a full anneal is used between stages and after severe cold work (8,9).

1.054 Grain growth in Type 321 can be expressed by $D^n - D_o^n = At \exp(-Q/RT)$, where D_o is the initial grain size, D is the grain size after an isothermal exposure at temperature T for a period t, Q is the activation energy, R is the gas constant, and n and A are constants. The exponent n for Type 321 has a best-fit value of 4. The activation energy is estimated as 100 ± 25 kcal/g mol. This large value of activation energy reflects grain-boundary pinning by carbides (45).

1.06 Hardness

1.061 Hardness of various forms, Table 1.061.

1.062 Effects of exposures to elevated temperatures on hardness at room temperature, Table 1.062.

1.063 Effect of cold rolling on hardness of strip, Table 1.063.

1.07 Forms and Conditions Available

Table 1.07.

1.08 Melting and Casting Practice

1.081 The alloy is normally air melted in electric-arc furnaces. For applications requiring exceptional quality, it can be induction or consumable-electrode remelted in vacuum.

1.082 The alloy can be cast as single ingots or continuous strands (46).

1.083 Grain refinement and more homogeneous carbide distribution can be effected by electromagnetic stirring during solidification (47).

1.09 Special Considerations

1.091 Solution annealing at temperatures above 1900 F results in partial dissolution of TiC, the extent of dissolution increasing with increasing annealing temperature. In the solution-annealed condition, the alloy can be subsequently sensitized by welding or by heating in the sensitization temperature range of about 800 to 1500 F. A stabilization anneal of 2 hours or longer at 1650 F after solution annealing is required to promote TiC precipitation and prevent subsequent sensitization (48).

1.092 Prolonged heating at 2000 F and above causes excessive grain growth.

1.0921 Effects of time and temperature on grain growth, Figure 1.0921.

1.093 Prolonged exposure in the temperature range 900 to 1500 F can significantly reduce room-temperature ductility and notched impact strength. See Tables 3.0213, 3.0214, 3.0231, and 3.0232.

1.094 In both the annealed and cold-worked conditions, a minimum in tensile ductility occurs in the temperature range 1100 to 1400 F. See Figures 3.0315, 3.0316, and 3.0319.

2 PHYSICAL AND CHEMICAL PROPERTIES

2.01 Thermal Properties

2.011 Melting range: 2500 to 2550 F (8), 2550 to 2600 F (9).

2.012 Phase changes.

2.0121 Time-temperature-transformation diagrams.

2.0122 The second phases in Type 321 vary with exposure time and temperature, prior thermomechanical history, and composition. In particular, the chemistries of the carbide phase(s) and hence the sensitization of the alloy to intergranular corrosion vary with aging conditions. After furnace aging of

Fe
18 Cr
10 Ni
+ Ti

Type 321

2000 F solution-annealed material for times up to 3000 hours at temperatures between 840 and 1740 F, $M_{23}C_6$ was determined as the major precipitating phase. However, after a service exposure of 17 years at 1050 to 1124 F, the major second phases were TiC and sigma. No $M_{23}C_6$ was observed in the service-exposed material, even though its chemistry was very similar to that of the furnace-aged material. It is suggested that TiC precipitate aligns into stringers during fabrication. On solution annealing, the precipitate dissolves and the carbon is well dispersed. However, the titanium, because of its lower diffusivity, remains in the vicinity of the original precipitate. During subsequent aging in the sensitization temperature range, the carbon near the titanium precipitates as TiC, while the remaining carbon reacts with the more abundant chromium to form $M_{23}C_6$ at the grain boundaries. Over a long time period, the $M_{23}C_6$ converts gradually to the more stable MC precipitate. Thus, while under equilibrium conditions enough titanium may be present to completely react with the carbon present, kinetic factors can permit the formation of metastable $M_{23}C_6$. The inclusion of a stabilization anneal at 1650 F after solution annealing will promote the formation of MC precipitate and prevent possible subsequent sensitization (49).

2.0123 Small amounts of sigma phase can form in Type 321 after long exposures at intermediate temperatures, depending on the chromium content. The critical chromium content for sigma formation in Type 321 has been established as 17.8 weight percent. At chromium contents above this value, sigma phase can form, while at lower levels it cannot. Sigma phase is detrimental to toughness and corrosion resistance. It can be removed by annealing (49).

2.0124 Sulfur in Type 321 precipitates as $Ti_4C_2S_2$ (49).

2.0125 Cold work transforms a small amount of austenite to ferrite.

2.013 Thermal conductivity, Figure 2.013.

2.014 Thermal expansion, Figure 2.014.

2.015 Specific heat. 0.12 Btu/(lb F) (8,33).

2.016 Thermal diffusivity.

2.02 **Other Physical Properties**

2.021 Density. 0.29 lb/in.^{3}, 8.0 g/cm^3 (8,33).

2.022 Electrical properties.

2.0221 Electrical properties at various temperatures, Table 2.0221.

2.023 Magnetic properties.

2.0231 In the annealed condition, Type 321 is practically nonmagnetic; the maximum permeability is 1.02 at 200H. Cold work induces a slight amount of magnetic permeability, which varies with the amount of cold work and the chemical composition (9).

2.0232 The Néel temperature for Type 321 is predicted as -420 to -360 F (50).

2.024 Emittance.

2.0241 Total normal emittance at elevated temperatures, Figure 2.0241.

2.025 Damping capacity.

2.03 **Chemical Environments**

2.031 General corrosion.

2.0311 Type 321 withstands ordinary rusting and is immune to all foodstuffs, sterilizing solutions, most organic chemicals and dyestuffs, and a wide variety of inorganic chemicals. It resists nitric acid well, halogen acids poorly, and sulfuric acids moderately. Although long-time exposure in the range 800 to 1600 F may lower its general corrosion resistance, it nevertheless maintains immunity to intergranular corrosion, which does occur in similarly exposed unstabilized grades of stainless steel (8,9,33).

2.0312 Type 321 is highly resistant to general corrosion and stress corrosion in contact with the dense hydrocarbon fuel RJ-5 (Shelldyne H) (25).

2.0313 It is susceptible to pitting, tunneling, and crevice types of corrosion in seawater, the susceptibility being greater near the surface of the ocean than at the bottom or at intermediate depths. The susceptibility of Type 321 to corrosion in seawater is less than that of Types 301 or 304, but greater than that of the higher chromium-nickel grades such as 309 and 310. Type 321, as well as most other stainless steels, is not recommended for long-time service in seawater unless protective measures are taken such as the application of an inert coating (26).

2.0314 Hydrochloric acid is highly aggressive to Type 321 and other stainless steels, since the protective surface oxide film normally present reacts with this chemical. Various organic additives inhibit the corrosion of Type 321 in hydrochloric acid, including hexamine [also known as hexamethylene-tetramine $(CH_2)_6N_4$]. As shown in Figure 2.0315, the corrosion rate of Type 321 in 1N HCl decreases with increasing hexamine concentration, with a maximum improvement of about 15-fold at 4 percent hexamine. Hexamine is effective over a range of acid concentrations from at least 1N to 10N, as shown in Figure 2.0316, and at temperatures up to 176 F, as shown in Figure 2.0317. The protection against corrosion is attributed to a chemisorbed passive film which prevents reaction of the alloy with the acid (51).

2.0315 Effects of hexamine on corrosion of Type 321 in 1N HCl, Figure 2.0315.

2.0316 Effects of hydrochloric acid concentration and hexamine on corrosion of Type 321, Figure 2.0316.

2.0317 Effects of temperature and hexamine on corrosion of Type 321 in hydrochloric acid, Figure 2.0317.

2.0318 The corrosion rate of Type 321 in sulfuric acid is reduced by the presence of small amounts of potassium iodide. The addition of 10^{-3} to 10^{-1}N KI is effective in inhibiting corrosion at sulfuric acid concentrations up to 15N, as shown in Figure 2.0319. However, at higher potassium iodide concentrations, localized pitting and perforation occur after 14 to 28 days' exposure, as indicated in Figure 2.03110. Increasing temperature increases the rate of corrosion. However, as shown in Figure 2.03111, inhibition by 10^{-3} to 10^{-1}N KI

Fe
18 Cr
10 Ni
+ Ti

Type 321

is effective up to at least 176 F. The reduced corrosion rates are attributed to chemisorption of a monolayer of the inhibitor, preventing corrosion on that fraction of the surface covered by the inhibitor (52).

2.0319 Effects of potassium iodide on sulfuric acid corrosion of Type 321, Figure 2.0319.

2.03110 Effects of potassium iodide and exposure time on corrosion weight loss in 1N sulfuric acid, Figure 2.03110.

2.03111 Effect of temperature and potassium iodide on corrosion of Type 321 in sulfuric acid, Figure 2.03111.

2.032 Intergranular corrosion.

2.0321 The intergranular corrosion behavior of Type 321 is greatly influenced by prior thermal history and its effect on distribution of carbon. In common with the unstabilized austenitic 18-8 stainless steels, solution-annealed Type 321 is sensitized by welding or by exposure in a critical temperature range, which causes precipitation of chromium-rich carbides at the grain boundaries. This precipitation depletes the chromium content of the matrix adjacent to the grain boundaries and, in turn, significantly decreases the local corrosion resistance. However, Type 321 contains titanium to preferentially react with free carbon and precipitate TiC rather than $Cr_{23}C_6$. The alloy can be stabilized so that it is not subject to sensitization. The corrosion rate of sensitized Type 321 increases with increasing solution-heat-treatment temperature as shown in Figure 2.0322. This change in corrosion rate is related to the change in amount of free carbon in solution after heat treatment. Solution annealing at 2192 F causes dissolution of most of the TiC so that the carbon is free to reprecipitate as $Cr_{23}C_6$ during subsequent sensitization. Initial heat treatments at lower temperatures, such as 1832 to 2066 F, leave a greater fraction of the carbon content tied up as TiC so that less chromium is removed by $Cr_{23}C_6$ precipitation. The nature of the TiC precipitate is also affected by solution-heat-treatment temperature. Above 1900 to 2000 F, the initial TiC is probably incoherent with the matrix and large enough to be stable. Below 1900 to 2000 F, the initial TiC forms on dislocations, is probably coherent, and is not large enough to be stable without further growth.

The corrosion behavior of solution-annealed alloy is also influenced by the temperature and time of the sensitization exposure, as shown in Figure 2.0323. At exposure times of less than 100 hours, sensitization occurs at 1022 and 1112 F because precipitation of $Cr_{23}C_6$ occurs more rapidly than precipitation of TiC However, at longer times, rehealing takes place through conversion of $Cr_{23}C_6$ to TiC with accompanying restoration of chromium to the depleted regions. At 1202 F, both $Cr_{23}C_6$ and TiC precipitate from the matrix, with subsequent gradual conversion of $Cr_{23}C_6$ to TiC. The corrosion rates in Figure 2.0323 reflect these changes in chromium content of the matrix, increasing as chromium is lost through precipitation of $Cr_{23}C_6$ and decreasing as chromium is restored by conversion of the precipitate to TiC.

The relationship between carbon content of the matrix and sensitization time and temperature for 18-8 type stainless steels is summarized by the C-curve in Figure 2.0324. At time-temperature combinations below the $M_{23}C_6$ nucleation line, the rate of $Cr_{23}C_6$ precipitation is too sluggish for sensitization to occur. However, at longer times and at temperatures up to about 1130 F, precipitation of $Cr_{23}C_6$ occurs in Type 321, depending on the free carbon content of the matrix. At temperatures above about 1130 F, as indicated by the dotted line, TiC precipitates concurrently with $Cr_{23}C_6$. After long times above 1200 F and short times above about 1600 F, only TiC is present and sensitization is avoided (53,54).

2.0322 Effects of high-temperature heat treatment on corrosion rate of Type 321, Figure 2.0322.

2.0323 Effects of sensitization reheating on corrosion rates of solution-annealed Type 321, Figure 2.0323.

2.0324 Time-temperature-dissolved carbon relationships for $Cr_{23}C_6$ precipitation and for stabilization in 18Cr-8Ni type stainless steels, Figure 2.0324.

2.0325 Cold work affects sensitization by enhancing diffusion and carbide precipitation rates. It also promotes finer and more uniformly distributed precipitate. Heavy cold work can improve the corrosion resistance of sensitized material, while lesser amounts of cold work can enhance sensitization and lead to transgranular corrosion. Hot fatigue cycling is seen to increase the corrosion rate as compared to material which was heat treated only (for similar time at the same temperature), as shown in Figure 2.0326 for Types 321 and 304. Type 321 is seen to have far superior corrosion resistance in all conditions as compared to Type 304. Although sensitization heat treatment increases the corrosion rates for both steels, the increase for Type 321 is less than that for Type 304. Deformation by fatigue at the sensitization temperature further reduces the corrosion resistance by increasing the amount of carbide precipitation (55).

2.0326 Effects of sensitizing heat treatment and fatigue cycling on corrosion behavior in boiling copper sulfate, Figure 2.0326.

2.0327 The heat-affected zone of fusion-welded material is subject to accelerated corrosion if the assembly is sensitized by aging or during exposure after welding. The susceptibility to localized corrosion is caused by a sensitization reaction similar to that which affects improperly solution-annealed and aged material, as described above in Paragraph 2.0321. During welding, material adjacent to the molten weld is heated sufficiently to dissolve most of the MC and $M_{23}C_6$ precipitates. Delta ferrite also forms in the matrix at this time. Rapid cooling after welding retards carbide reprecipitation. During subsequent aging at about 1020 to 1560 F, chromium-rich $M_{23}C_6$ precipitates at the gamma grain boundaries and in the delta ferrite, decreasing the chromium content of these regions and causing sensitization. Some MC-type carbides also

Fe
18 Cr
10 Ni
+ Ti

Type 321

precipitate during aging, but insufficient carbon is tied up as MC to prevent precipitation of $M_{23}C_6$. The localized increased corrosion in the weld heat-affected zone is termed knife-line attack because of the sharp boundary line between corrosion-resistant and non-corrosion-resistant material. As seen in Figure 2.0328, the localized corrosion rate is maximized after an exposure of about 50 hours at 1202 F. At longer exposure times, the corrosion resistance improves, probably due to desensitization (rehealing) by conversion of the precipitate from $M_{23}C_6$ to MC. The corrosion resistance also improves with increasing welding heat input. Accelerated knife-line attack can be considerably reduced by a stabilization heat treatment of 2 hours at 1650 F after welding. This stabilization heat treatment ties up the carbon by precipitation as MC, reducing the loss of chromium as $M_{23}C_6$ during subsequent lower temperature aging. Knife-line-attack sensitivity in Type 321 can also be reduced by alloying with about 0.11 weight percent mischmetal, which accelerates precipitation of MC-type carbides. This level of mischmetal addition has no significant adverse effect on tensile properties (56–60).

2.0328 Effects of aging time on knife-line corrosion rate of arc-welded alloy, Figure 2.0328.

2.033 Stress corrosion.

2.0331 Austenitic stainless steels are particularly susceptible to stress-corrosion cracking as compared to the martensitic (400 series) and ferritic (430 series) stainless steels. Chloride-containing media are most corrosive and austenitic stainless steel components must be entirely stress-free for use in chloride-containing environments (61).

2.0332 Stress-corrosion crack-growth rates as a function of stress-intensity factor for Types 321, 304, 304L, and 316L in hot NaCl solutions are compared in Figure 2.0333. All four alloys exhibit a threshold stress-intensity factor below which no cracking occurs. As the stress-intensity factor increases above the threshold, the crack-growth rate increases sharply to a plateau rate of between 10^{-5} and 10^{-6} in./min. The threshold stress-intensity factor for Type 321 is higher than those for Types 304L and 316L but lower than that for solution-annealed Type 304. The stress-corrosion cracking of iron-nickel-chromium alloys is largely determined by nickel content, as shown in Figure 2.0334. Minimum corrosion resistance is exhibited by alloys containing 10 to 25 percent nickel. Alloys containing more than 25 percent nickel are resistant to chloride stress corrosion, while those containing less than 10 percent tend to be more corrosion resistant but are affected by heat treatment. For example, sensitized Type 304 has a substantially lower threshold stress-intensity factor than that for annealed Type 304. Type 321, being stabilized by titanium, does not exhibit the intergranular stress-corrosion cracking which occurs with sensitized Type 304, but rather shows transgranular cracking which is typical of unsensitized alloys (62).

2.0333 Effect of stress-intensity factor on stress-corrosion crack-growth rate in hot NaCl solution for Type 321 and three other austenitic stainless steels, Figure 2.0333.

2.0334 Effect of nickel content on threshold stress intensity for corrosion cracking in hot NaCl solution for iron-nickel alloys containing about 18 percent chromium, Figure 2.0334.

2.0335 The corrosion resistance of Type 321 weldments can be improved by shot peening. An unpeened welded assembly cracked severely after 22-hour immersion in boiling $MgCl_2$, while a similar peened assembly showed no stress-corrosion cracking after 264 hours (80).

2.0336 Type 321 is resistant to stress-corrosion cracking in seawater, but it is susceptible to both stress corrosion and pitting corrosion in marine atmospheric environment such as seashores and aboard ship. Zinc-rich and aluminum-rich coatings are effective in preventing or retarding the corrosion; surface treatments, such as electropolishing and chemical passivation, are less effective (27).

2.034 Hydrogen embrittlement.

2.0341 A modest degree of low-temperature hydrogen embrittlement is exhibited by Type 321 during tensile testing. This embrittlement occurs in material which has been sensitized by heat treatment prior to cathodic hydrogen charging. The degree of embrittlement at -321 F increases with increasing sensitization time at 1472 F, as shown in Figure 2.0342. The degree of embrittlement by hydrogen also increases with increasing solution-annealing temperature, as shown in Figure 2.0343. Type 321 is more resistant to low-temperature hydrogen embrittlement than the standard grades of Types 304 and 316 but less resistant than the low-carbon modifications of these two alloys and Types 310 and 347 (63).

2.0342 Effects of hydrogen charging and sensitization on tensile ductility at -321 F, Figure 2.0342.

2.0343 Effects of solution-annealing temperature on elongation ratio at -321 F for Type 321 and six other austenitic stainless steels, Figure 2.0343.

2.0344 Type 321 suffers hydrogen embrittlement at room temperature when cathodically charged with hydrogen during tensile testing. As shown in Figure 2.0345, embrittlement under these conditions is observed both in the solution-annealed condition and after sensitization heat treating. Large-grained material is slightly more susceptible to embrittlement than finer grained material (64).

2.0345 Effects of grain size and heat treatment on hydrogen embrittlement during tensile testing at room temperature, Figure 2.0345.

2.0346 Type 321 is subject to hydrogen-induced slow crack growth when charged under load, as shown in Figure 2.0347. Slow crack growth also occurs when precharged specimens are tested in air at stress intensities near the plane-strain fracture toughness. However, hydrogen outgasses at room temperature in about 10 hours, so that material which does not fail in shorter times then does not fail by hydrogen embrittlement. Slow crack growth does not occur at any stress if precharged specimens are outgassed before testing. The fracture mode changes from ductile tearing to brittle quasi-cleavage as the stress intensity is decreased under hydrogen-embrittlement conditions (65,66).

2.0347 Effects of hydrogen charging on delayed failure behavior of Type 321, Figure 2.0347.

2.0348 Exposure to hydrogen at a pressure of 2900 psi and 1112 F for 20 days causes hydrogen attack in Type 321. This attack is in the form of internal bubbles containing methane, ethane, and hydrogen, which form at $M_{23}C_6$, and MC carbide particles. The effects of these bubbles on mechanical properties have not been reported (67).

2.0349 At room and cryogenic temperatures, hydrogen at a pressure of 5000 psi has no significant effect on smooth or notched tensile properties, as shown later in Table 3.03711.

2.035 Oxidation.

2.0351 Type 321 oxidizes more rapidly in air at 1742 F than Types 304, 310, and 316, as shown in Figure 2.0352. The scale formed on Type 321 spalls on cooling, while scales on Types 310 and 316 remain adherent if the alloys are slow cooled after oxidation exposure. Internal oxidation is also noted in Type 321, particularly after several cycles of oxidation exposure (68).

Type 321 can be used in air at temperatures up to 1600 F without excessive scaling (8,11,33).

2.0352 Oxidation weight-change behavior of Type 321 in air at 1742 F as compared to Types 304, 310, and 316, Figure 2.0352.

2.036 Liquid-metal corrosion.

2.0361 Type 321 is suitable for the containment of liquid cesium and rubidium for possible application in liquid-metal-cooled nuclear reactors. It is less suitable for potassium and lithium (28).

2.04 **Nuclear Environments**

2.041 Neutron irradiation increases the strength and reduces the ductility of Type 321. The effect on strength is pronounced at test temperatures up to 1100 F, but decreases with further increases in temperature with full recovery occurring at about 1500 F. The marked deterioration in ductility, however, persists to at least 1500 F (23).

2.042 Effects of fast-neutron irradiation on tensile properties at elevated temperatures, Table 2.042.

2.043 Ion-bombardment results indicate that austenitic stainless steels such as Type 321 tend to swell large amounts under conditions such as would be encountered in a liquid-metal fast-breeder reactor (69).

3 MECHANICAL PROPERTIES

3.01 **Specified Mechanical Properties**

3.011 AMS specified mechanical properties, Table 3.011.

3.02 **Mechanical Properties at Room Temperature**

3.021 Tension – stress-strain diagrams – tension properties.

3.0211 Stress-strain curves (see Figures 3.0311 through 3.0314).

3.0212 Tensile properties of various forms, Table 3.0212.

3.0213 Effects of 100,000-hour exposures to elevated temperatures on room-temperature tensile properties, Table 3.0213.

3.0214 Effects on room-temperature tensile properties of elevated-temperature exposures under load, Table 3.0214.

3.0215 Tensile properties of extrusions, Table 3.0215.

3.0216 Effect of carburizing on room-temperature tensile properties, Figure 3.0216.

3.022 Compression – stress-strain diagrams – compression properties.

3.0221 Stress-strain curves (see Figure 3.0321).

3.0222 Compressive yield strength (see Figure 3.0322).

3.023 Impact.

3.0231 Effects of exposures to elevated temperatures on room-temperature impact properties, Table 3.0231.

3.0232 Effects on room-temperature impact properties of elevated-temperature exposures under load, Table 3.0232.

3.024 Bending.

3.025 Torsion and shear (see Figure 3.0351).

3.026 Bearing (see Figure 3.0361).

3.027 Stress concentration.

3.0271 Notch properties (see Table 3.03711).

3.0272 Fracture toughness.

3.028 Combined properties.

3.03 **Mechanical Properties at Various Temperatures**

3.031 Tension – stress-strain diagrams – tension properties.

3.0311 Stress-strain curves for sheet at room and elevated temperatures, Figure 3.0311.

3.0312 Complete stress-strain curves for sheet at room and elevated temperatures, Figure 3.0312.

3.0313 Stress-strain curves for sheet at room and low temperatures, Figure 3.0313.

3.0314 Complete stress-strain curves for bar at room and low temperatures, Figure 3.0314.

3.0315 Scatter bands for tensile properties of bar at room and elevated temperatures, Figure 3.0315.

3.0316 Effect of elevated temperatures on tensile properties of sheet, Figure 3.0316.

3.0317 Effects of low temperatures on tensile properties of bar and sheet, Figure 3.0317.

3.0318 Effects of cold work induced by hydraulic expansion on tensile properties of tubing at 70 F and -320 F, Figure 3.0318.

3.0319 Effects of temperature on tensile properties of annealed and cold-rolled bar, Figure 3.0319.

3.03110 Effects of temperature, after two different exposure times at temperature, on tensile properties of sheet, Figure 3.03110.

3.03111 Effects of temperature, rapid strain rates, and short holding times at temperature on tensile properties of sheet heated to test temperatures within 10 seconds, Figure 3.03111.

3.03112 Effects of temperature on tensile properties of bar annealed at various temperatures, Figure 3.03112.

3.032 Compression – stress-strain diagrams – compression properties.

3.0321 Compressive stress-strain curves for sheet at room and elevated temperatures, Figure 3.0321.

3.0322 Effects of temperature, after two different exposure times at temperature, on compressive yield strength of sheet, Figure 3.0322.

3.033 Impact.

3.034 Bending.

3.035 Torsion and shear.

3.0351 Effects of temperature, after two different exposure times at temperature, on shear strength of sheet, Figure 3.0351.

3.036 Bearing.

Fe
18 Cr
10 Ni
+ Ti

Type 321

Fe
18 Cr
10 Ni
+ Ti

Type 321

3.0361 Effects of temperature, after two different exposure times at temperature, on bearing properties of sheet, Figure 3.0361.

3.037 Stress concentration.

3.0371 Notch properties.

3.03711 Smooth and notched tensile properties in high-pressure helium and hydrogen at 70 F and -200 F, Table 3.03711.

3.0372 Fracture toughness.

3.038 Combined properties.

3.04 **Creep and Creep Rupture Properties**

3.041 Effect of temperature on creep-rupture strength, Figure 3.041.

3.042 Creep and creep-rupture curves for sheet at 1200 and 1500 F, Figure 3.042.

3.043 Creep curves for sheet at 1000 to 1350 F, Figure 3.043.

3.044 Creep rates for sheet at 1000 to 1350 F, Figure 3.044.

3.045 Short-time total-strain curves for sheet at 1500 and 1800 F, Figure 3.045.

3.046 Creep-rupture curves for bar at 1100 to 1500 F, Figure 3.046.

3.047 Effects of annealing temperature and cold work on creep-rupture properties at 1200 F, Figure 3.047.

3.05 **Fatigue Properties**

3.051 Type 321 exhibits cyclic strain hardening at room temperature to 1292 F, as shown by comparison of the cyclic and monotonic stress-strain curves in Figure 3.052 (70).

3.052 Monotonic and cyclic stress-strain curves for bar at room and elevated temperatures, (a) room temperature, (b) 842 F, (c) 1112 F, (d) 1292 F, Figure 3.052.

3.053 Low-cycle fatigue life at room and elevated temperatures, Figure 3.053.

3.054 High-cycle fatigue strength at room and elevated temperatures, Figure 3.054.

3.055 Fatigue properties of air-melted and vacuum-melted sheet, Figure 3.055.

3.056 The effects of thermal aging on fatigue behavior at 1112 and 1292 F are shown in Figure 3.057. At a cyclic strain rate of 40 percent/min, there is minimal effect of thermal aging on fatigue life. The fracture surface is transgranular and well-defined striations are observed. At a cyclic strain rate of 0.4 percent/min, thermal aging increases the fatigue life, with the effect being greater at 1292 F than at 1112 F. The fracture mode at the lower cyclic strain rate is intergranular. The improvement in fatigue life by aging is attributed to large chromium carbide precipitate particles at the grain boundaries which inhibit grain-boundary sliding (74).

3.057 Effects of aging and cyclic strain rate on fatigue behavior at elevated temperatures, (a) 1112 F, (b) 1292 F, Figure 3.057.

3.058 The effect of cyclic frequency on low-cycle fatigue behavior increases with increasing temperature. As shown in Figure 3.059, little effect of frequency is apparent at room temperature and at 842 F. However, at 1112 to 1472 F, the fatigue life is notably shorter at a cyclic strain rate of 0.4 percent/min than at 40 percent/min. This decreased fatigue life is attributed to a greater creep component of fatigue at the lower frequency (70,73). Surface cracks show a greater tendency to propagate intergranularly with increasing temperature, decreasing cyclic strain rate, and increasing strain range (75).

3.059 Low-cycle axial fatigue behavior in air at room and elevated temperatures, Figure 3.059, (a) room temperature, (b) 842 F, (c) 1112 F, (d) 1292 F, (e) 1472 F.

3.0510 Fatigue life at 1112 F is affected by grain size at a cyclic strain rate of 0.4 percent/min but not at a cyclic strain rate of 40 percent/min, as shown in Figure 3.0511. The fracture mode is also affected by strain rate and grain size. At the higher cyclic strain rate, fracture is transgranular with a striated fracture surface. However, at the lower cyclic strain rate, the fracture mode changes from primarily transgranular at a grain size of 9 (small grain size) to completely intergranular at a grain size of 1 (large grain size). The fatigue lives of Type 321 and seven other austenitic stainless steels at 1112 F are compared in Figure 3.0512. The effect of composition is minor as compared to the effects of grain size and cyclic strain rate. At a cyclic strain rate of 40 percent/min, grain size has no effect on any of these alloys. At a cyclic strain rate of 0.4 percent/min, the fatigue life is decreased at smaller grain size numbers. When a tensile hold time of 30 minutes is incorporated into the fatigue cycle, the fatigue life is further reduced. Fracture under these conditions is completely intergranular at all grain sizes and the intergranular mode becomes more distinct with decreasing grain-size number. Similar behavior is also observed at 1292 F (76).

3.0511 Effects of grain size and cyclic frequency on axial fatigue behavior at 1112 F, Figure 3.0511.

3.0512 Effects of grain size, cyclic frequency, and hold time on axial fatigue life of austenitic stainless steels at 1112 F, Figure 3.0512.

3.0513 At room temperature and 842 F, the fatigue life of electropolished material is about twice that of as-machined material, as shown in Figure 3.0514. At 1292 F, no effect of surface finish is observed. The shorter life of the as-machined material at room temperature and 842 F is attributed to the presence of a work-hardened surface layer which allows earlier crack initiation than does a stress-free (electropolished) surface. At room temperature and 842 F, surface cracks are initiated at twin boundaries, while at 1292 F, they initiate at grain boundaries (75).

3.0514 Effect of surface finish on axial fatigue behavior at room and elevated temperatures, Figure 3.0514.

3.0515 Effects of low temperatures and surface finish on fatigue properties, Figure 3.0515.

3.0516 Fatigue crack-growth rate as a function of stress-intensity-factor range at various temperatures, Figure 3.0516.

3.0517 Thermal aging decreases the fatigue crack-propagation rate at 1100 F, as shown in Figure 3.0518. The incorporation of 0.1- and 1-minute hold times increases the crack-propagation rate in the aged condition (77).

3.0518 Effects of aging and cyclic hold time on bending-fatigue crack-growth rate at 1100 F, Figure 3.0518.

3.0519 Under conditions where the fatigue stress is above the yield stress and a linear elastic fracture mechanics treatment is not applicable, the fatigue crack-growth rate can be represented as a function of crack length. As shown in Figure 3.0520, the crack-growth rate increases with increasing total strain range at 1112 F. The crack-growth rate also increases with decreasing cyclic strain rate (frequency) and is decreased by aging. Increasing temperature slightly increases the crack-growth rate. The fatigue life is inversely dependent on the crack-growth rate, as shown in Figure 3.0521. This relationship also indicates that fatigue life is related inversely to those variables which affect the fatigue crack-growth rate (78).

3.0520 Relation between crack-growth rate and crack length at room and elevated temperatures, (a) room temperature and 842 F, (b) 1112 F, (c) 1292 F, Figure 3.0520.

3.0521 Relation between fatigue life and crack-propagation rate, Figure 3.0521.

3.0522 The room-temperature yield strength after high-cycle fatigue is initially increased by flow stress hardening, but eventually decreases to a value approximately equal to that of the cyclic stress level applied. This behavior is shown in Figure 3.0523 (71).

3.0523 Effect of axial fatigue on subsequent yield strength at room temperature, Figure 3.0523.

3.06 **Elastic Properties**

3.061 Poisson's ratio.

3.0611 Effect of temperature on Poisson's ratio, Figure 3.0611.

3.062 Modulus of elasticity.

3.0621 Modulus of elasticity at room and elevated temperatures, Figure 3.0621.

3.0622 Modulus of elasticity at low temperatures, Figure 3.0622.

3.0623 Tangent modulus curves in compression, Figure 3.0623.

3.063 Modulus of rigidity.

3.0631 Modulus of rigidity at room and elevated temperatures, Figure 3.0631.

4 FABRICATION

4.01 **Forming**

4.011 In the annealed condition, Type 321 is sufficiently tough and ductile to be cold formed by most commercial methods, such as deep drawing, bending, and upsetting. Since it work hardens rapidly, intermediate process anneals or full anneals may be necessary for severely cold-worked parts (8,33).

4.012 It has good hot-forming characteristics by any of the conventional methods, such as forging, rolling, extrusion, and upsetting. Because of its higher hot hardness, more power for a given reduction is required than with mild steel. High-sulfur fuels and strongly reducing atmospheres should be avoided. The material to be hot formed should be preheated to 1500 to 1600 F and then hot formed in the range 2300 to 1700 F. Air cooling after hot forming is usually adequate to retain good corrosion resistance (8,11,33).

4.013 Austenitic stainless steels, such as Type 321, are usually extruded in the range 2100 to 2250 F It is essential that the extrusion billet is lubricated both at the billet/liner interface and at the billet/die interface in order to achieve acceptable low extrusion pressures and good extrusion surface quality. Soda lime and borosilicate glasses are used for this purpose. Inadequate or uneven lubrication can result in transverse cracking, tearing, or surface roughness. The surface quality of properly extruded products can be better than that obtained by hot rolling, especially in the case of shapes. Extrusion pressures for Type 321 as a function of temperature, ram speed, and extrusion ratio are shown in Figure 4.014 (79).

Fe
18 Cr
10 Ni
+ Ti
Type 321

4.014 Effects of extrusion ratio, reheat temperature, and ram speed on peak extrusion pressure, Figure 4.014.

4.02 **Machining and Grinding**

4.021 Because of its toughness and work-hardening characteristics, Type 321 requires rigid machine setups and sharp tools. Better chip action on chip-breaker tools and a better finish are obtained with moderately cold-worked material than with annealed. Heavy feeds and an adequate supply of coolant are recommended. In general, it is machined at speeds about 45 percent of those used for free-machining AISI B1112 steel. In turning operations, speeds of 50 to 90 sfm can be used. (8,33).

4.03 **Joining**

4.031 Type 321 is readily welded by the various electric-arc, oxyacetylene, resistance, and electron-beam methods. Since titanium tends to be lost during welding, another stabilized grade of stainless steel, Type 347, is recommended for electrodes and filler wire. Weldments should be stabilization heat treated to prevent possible subsequent sensitization and intergranular corrosion. Type 321 has low susceptibility to weld-metal hot cracking (8,33,55–60,81).

4.0311 Tensile properties of specimens butt welded in vacuum by low-voltage and high-voltage electron-beam processes; no preheat or postheat treatments, Table 4.0311.

4.032 Type 321 can be brazed with various nickel-base, copper-base, and exotic brazing alloys, such as 82 percent gold-18 percent nickel. Vacuum or hydrogen brazing atmospheres are desirable (18).

4.0321 Shear strength of brazed joints, Table 4.0321.

4.04 **Surface Treatment**

4.041 Because of its inherent good corrosion resistance, protective coatings and surface treatments are not normally needed for Type 321. Nevertheless, improved corrosion resistance when needed can be obtained by coating, preferably with zinc- or aluminum-rich paints or by passivating for 20 to 30 minutes in a warm solution of 20 percent (volume) nitric acid to which 3 ounces per gallon of sodium dichromate has been added (27,33).

Fe
18 Cr
10 Ni
+ Ti

Type 321

4.042 For optimum corrosion resistance the surface must be free of scale and foreign metallic contaminants. Preferred cleaning treatments are either mechanical methods such as buffing, sandblasting, or vapor blasting, or scale conditioning in a molten caustic salt bath followed by light acid pickling.

4.043 Type 321 can be satisfactorily cleaned of oxide by pickling in a mixed solution of nitric acid and hydrofluoric acid at 120 to 140 F. The bath composition varies, depending on the thickness of the scale, ranging from 10 to 25 percent nitric acid and 1 to 4 percent hydrofluoric acid. The ratio of nitric acid to hydrofluoric acid is decreased for thicker scales (85).

4.044 Type 321 can be surface hardened by nitriding or boronizing for improved wear resistance. Figure 4.045 shows the extent of hardening by nitriding for 24 hours at 1020 to 1560 F in a $90NH_3$-$10N_2$ mixture at atmospheric pressure and also by pack boronizing. A layer of M_4N is formed at the surface by nitriding at 1020 to 1380 F, while a mixture of M_4N and M_2N is formed at 1560 F. Very good wear characteristics are exhibited by Type 321 nitrided at 1220 F. Pack-boronizing with a commercial compound containing boron carbide produced a hard but thinner surface layer than that obtained by nitriding. The outer portion of the surface was an alloy boride with stoichiometry corresponding to MB, while the inner portion of the layer corresponded to M_2B. The wear resistance of boronized Type 321 was not evaluated but would be expected to be good based on results obtained with pack-boronized Type 316 (82,83).

4.045 Hardness-depth profiles for Type 321 after nitriding at 1020 to 1560 F or boronizing at 1740 F, Figure 4.045.

4.046 Type 321 can also be hard-coated by liquid-phase-sintering of Ni-Cr-B-Si powder mixtures onto the substrate. The smoothness of the coating surface is better than that obtained with thermospraying and subsequent melting techniques (84).

REFERENCES

1 Aerospace Material Specification, AMS 5510M (April 1, 1983).

2 Aerospace Material Specification, AMS 5557F (January 1, 1983).

3 Aerospace Material Specification, AMS 5559E (January 1, 1983).

4 Aerospace Material Specification, AMS 5570L (January 1, 1983).

5 Aerospace Material Specification, AMS 5576G (April 1, 1983).

6 Aerospace Material Specification, AMS 5645L (April 1, 1983).

7 Aerospace Material Specification, AMS 5689C (April 1, 1983).

8 "Uniloy 321/347/348 Stainless Steels", Universal-Cyclops, Specialty Steel Division (1966).

9 "Stainless Steel Types 347, 348, and 321", Allegheny-Ludlum Steel Corp. Blue Sheet (1970).

10 "Armco Stainless Steels", Armco Steel Corp., Bulletin LA-172 (1972).

11 "Steels for Elevated Temperature Service", U.S. Steel Corporation (June 1972).

12 "Fatigue Properties of Air-Melted and Consutrode-Melted Type 321", Allegheny-Ludlum, Data Sheet 135-121859-321.

13 Schmidt, E. H., and Green, E. F., "Fatigue Properties of Sheet, Bar and Cast Metallic Materials for Cryogenic Applications", Rocketdyne R-7564 (August 1968).

14 "Mechanical Test Results on Various Extruded Materials", Allegheny-Ludlum (January 1, 1956).

15 Stanley, J. K., and Perrotta, A. J., "Grain Growth in Austenitic Stainless Steels", *Metallography*, Vol 2 (December 1969).

16 Stanley, J. K., "Mechanical Properties of Carburized Austenitic Stainless Steels as Related to Microstructure", Aerospace Corporation, Report No. TR-0066(5250-10)-1 (July 1969).

17 "Resumé of Investigations for High-Temperature, High Pressure Applications 1960–1962", Timken Roller Bearing Company (1962).

18 Fazio, F., "Gold-Nickel Eutectic Filler Metal for Brazing Iron, Nickel and Cobalt Base Alloys", Boeing Report No. MDR 2-33008 (March 1971).

19 Mischel, H. T., "Optimum Materials for Ducting Flexible Components", Solar Div. ER 1925 (December 1967).

20 Burrows, C. F., "Manufacturing Methods and Technology Study Covering Parameters for the Application of Electron-Beam Welding", Martin Marietta Corporation Report No. IE-TR-69-5 (August 1969).

21 Stanley, J. K., "Effect of Silicon Additions on the Carburization Resistance, Mechanical Properties, and Joining Characteristics of Stabilized Austenitic Stainless Steels", Aerospace Corporation, Report No. TR-0172 (2250-10)-4 (November 15, 1971).

22 Steels, L. E., et al., "Irradiation Effects on Reactor Structural Materials", Naval Research Lab Memorandum Report 2398 (February 15, 1972).

23 Lauritzen, T., Withop, A., and Ferguson, G. P., "Mechanical Properties Evaluation of Austenitic Stainless Steels Irradiated in EBR-II", General Electric, Report GEAP 10066 (July 1969).

24 "Emissivity of Metals at Elevated Temperatures", McDonnell Aircraft Corporation, Report 9069, Serial No. 28 (October 1962).

25 Sargent, D. H., and Bielawski, C., "Advanced Fuel Systems for Ramjet-Powered Vehicles", Atlantic Research Corporation, TR-PL-9870-03 (March 1970).

26 Reinhard, F. M., "Corrosion of Materials in Hydrospace, Part VI, Stainless Steels", Naval Civil Engineering Lab TN N-1172 (September 1971).

27 Morrison, J. D., "Corrosion Study of Bare and Coated Stainless Steel", Kennedy Space Flight Center, NASA TN D-6519 (July 1972).

28 Phillips, W., "Effects of Alkali Metal Gettering Agents on Stainless Steel Corrosion", Jet Propulsion Lab, TR32-1239 (April 1, 1968).

29 Walker, R. J., "Influence of Gaseous Hydrogen on Metals", Rocketdyne Report N71-32489 (May 24, 1971).

30 Military Standardization Handbook, Cross Index of Chemically Similar Specifications, MIL-HDBK-H1D (June 22, 1970).

31 Metal Progress, 1974 Databook, Vol 106 (June 1974).

32 Carden, A. E., McEvily, A. J., and Wells, C. H., "Fatigue at Elevated Temperatures", ASTM STP 520 (June 1972).

33 "Carpenter Stainless Type 321", Carpenter Technology Corporation (1970).

34 "Stainless Steel Type 321", North American Aviation Summary Report AL-2604 (October 30, 1957).

35 "Digest of Steels for High-Temperature Service", Timken Roller Bearing Co., Sixth Edition (1957).

36 Miller, D. E., "Determination of the Physical Properties of Ferrous and Non-Ferrous Structural Sheet Materials at Elevated Temperatures", AFTR 6517, Pt. 4 (December 1954).

37 Dedman, H. E., Wheelahan, E. J., and Kattus, J. R., "Tensile Properties of Aircraft-Structural Metals at Various Rates of Loading After Rapid Heating", WADC TR58-440, Part 1 (November 1958).

38 Durham, T. F., McClintock, R. M., and Reed, R. P., "Cryogenic Materials Data Handbook", U.S. Dept. of Commerce (1960).

39 Simmons, W. F., and Cross, H. C., "Report on the Elevated-Temperature Properties of Stainless Steels", ASTM STP 124 (January 1952).

40 Dotson, C. L., and Kattus, J. R., "Tensile Properties of Aircraft-Structural Materials at Various Rates of Loading After Rapid Heating", WADC TR55-199, Pt. 1 (August 1955).

41 Perlmutter, I., "Stress-Rupture Tests on Sheet Alloys for High-Temperature Applications", AFTR No. 6188 (July 1950).

42 Perlmutter, I., and Rector, W. H., "Investigation of Sheet Materials for Application at High Temperatures", AFTR No. 5712 (July 13, 1948).

43 Van Echo, J. A., Worth, W. F., and Simmons, W. F., "Short-Time Creep Properties of Structural Sheet Materials for Aircraft and Missiles", AFTR No. 6731, Pt. III (May 1955).

44 Garofalo, F., Malenock, P. R., and Smith, G. V., "The Influence of Temperature on Elastic Constants of Some Commercial Steels", Symposium on Determination of Elastic Constants, ASTM STP 129 (June 25, 1952).

45 German, R. M., "Grain Growth in Austenitic Stainless Steels", *Metallography*, Vol 11, No. 2 (April 1978), pp 235–239.

46 Nakano, Y., Noguchi, Y., Hoshi, F., and Muranaka, Y., "Continuous Casting of Stainless Steel Slabs", *Ironmaking and Steelmaking*, Vol 4, No. 6 (1977), pp 361–367.

47 Takeuchi, H., Ikehara, Y., Yanai, T., and Matsumura, S., "Quality Improvement of Continuously Cast Stainless Steel Blooms Through Electromagnetic Stirring", *Journal of the Iron and Steel Institute of Japan*, Vol 63, No. 8 (July 1977), pp 1287–1296.

48 Hotaling, A. C., and Scharfstein, L. R., "The Effect of Heat Treatments in the Prevention of Intergranular Corrosion Failures of AISI 321 Stainless Steel", *Materials Performance*, Vol 22, No. 9 (September 1983), pp 22–24.

49 Leitnaker, J. M., and Bentley, J., "Precipitate Phases in Type 321 Stainless Steel After Aging 17 Years at Approximately 600 C", *Metallurgical Transactions*, Vol 8A, No. 10 (October 1977), pp 1605–1613.

50 Warnes, L.A.A., and King, H. W., "The Low Temperature Magnetic Properties of Austenitic Fe-Cr-Ni Alloys – 2. The Prediction of Neel Temperatures and Maximum Susceptibilities", *Cryogenics*, Vol 16, No. 11 (November 1976), pp 659–667.

51 Pandey, G. N., and Sanyal, B., "Inhibition of the Corrosion of Stainless Steel (AISI 321) in Hydrochloric Acid", *Corrosion Prevention and Control*, Vol 27, No. 3 (June 1980), pp 13–17.

52 Gupta, S., Pandey, G. N., and Sanyal, B., "Effect of Potassium Iodide on the Attack of Stainless Steel by Sulfuric Acid", *Metal Finishing*, Vol 80, No. 8 (August 1982), pp 51–54.

53 Samans, C. H., Kinoshita, K., and Matsushima, I., "Further Observations on Sensitization of Chemically Stabilized Stainless Steels", Vol 33, No. 8 (August 1977), pp 271-279.

54 Samans, C. H., Kinoshita, K., and Matsushima, I., "Sensitization and Stabilization of Type 321 Stainless Steels", presented at Corrosion/75, Toronto, Canada (April 14–18, 1975), pp 4/1–4/11.

55 Hoffman, C., and McEvily, A. J., "The Effect of High Temperature Low Cycle Fatigue on the Corrosion Resistance of Austenitic Stainless Steels", *Metallurgical Transactions*, Vol 13A, No. 5 (May 1982), pp 923–927.

56 Ikawa, H., Shin, S., Nakao, Y., and Nishimoto, K., "Knife Line Attack Phenomenon in Stabilized Stainless Steels – Effect of Heat Treatment on Knife Line Attack Phenomenon", *Technical Reports of the Osaka University*, Vol 25 (October 1975), pp 337–345.

57 Ikawa, H., Shin, S., Nakao, Y., and Nishimoto, K., "Knife Line Attack Phenomenon in Stabilized Stainless Steels – Mechanism of Knife Line Attack Phenomenon II", *Technical Reports of the Osaka University*, Vol 26 (October 1976), pp 427–435.

58 Ikawa, H., Shin, S., Nakao, Y., and Nishimoto, K., "Knife Line Attack Phenomenon in Stabilized Stainless Steels – Dissolution Phenomenon of Carbides in Thermal Cycles", *Technical Reports of the Osaka University*, Vol 27 (October 1977), pp 381–388.

59 Ikawa, H., Nakao, Y., and Nishimoto, K., "Knife Line Attack Phenomenon in Stabilized Stainless Steels – Precipitation Phenomenon of Carbides During Post-Heat Treatment", *Technical Reports of the Osaka University*, Vol 28 (March 1978), pp 67–74.

60 Ikawa, H., Nakao, Y., and Nishimoto, K., "Improvement of Knife Line Attack Phenomenon in Stabilized Stainless Steels by Addition of REM", *Technical Reports of the Osaka University*, Vol 28 (March 1978), pp 75–83.

61 Keys, L. H., "The Corrosion of Stainless Steels", *Australasian Corrosion Engineering*, Vol 20, No. 3 (March 1976), pp 9–16.

62 Speidel, M. O., "Stress Corrosion Cracking of Stainless Steels in NaCl Solutions", *Metallurgical Transactions*, Vol 12A, No. 5 (May 1981), pp 779–789.

Fe
18 Cr
10 Ni
+ Ti

Type 321

Fe
18 Cr
10 Ni
+ Ti

Type 321

63 Kuribayashi, M., Okabayashi, H., "The Influence of Heat-Treatment and Cold-Work on the Low Temperature Hydrogen Embrittlement of Austenitic Stainless Steels", *Journal of the Japan Institute of Metals*, Vol 47, No. 4 (April 1983), pp 365–372.

64 Rozenak, P., and Eliezer, D., "Effects of Metallurgical Variables on Hydrogen Embrittlement in AISI Type 316, 321 and 347 Stainless Steels", *Materials Science and Engineering*, Vol 61, No. 1 (October 1983), pp 31–41.

65 Eliezer, D., Arbel, A., and Rozenak, P., "Hydrogen Induced Delay Failure of AISI 316L and 321 Types Stainless Steels", *Journal of Materials Science Letters*, Vol 2, No. 10 (October 1983), pp 602–604.

66 Chu, W-Y., Yao, J., and Hsiao, C-M., "Hydrogen Induced Slow Crack Growth in Stable Austenitic Stainless Steels", *Metallurgical Transactions*, Vol 15A, No. 4 (April 1984), pp 729–733.

67 Yacaman, M. J., Parthasarathy, T. A., and Hirth, J. P., "Hydrogen Attack in an Austenitic Stainless Steel", *Metallurgical Transactions*, Vol 15A (September 1984), pp 1485–1490.

68 Moccari, A., and Ali, S. I., "Studies on the Oxidation and Spalling Resistance of Austenitic Stainless Steels", *British Corrosion Journal*, Vol 14, No. 2 (1979), pp 91–96.

69 Johnston, W. G., Lauritzen, T., Rosolowski, J. H., and Turkalo, A. M., "Void Swelling in Fast Reactor Materials – A Metallurgical Problem", *Journal of Metals*, Vol 28, No. 6 (June 1976), pp 19–24.

70 Yamaguchi, K., Kanazawa, K., and Yoshida, S., "Dependence of Temperature and Strain Rate on the Low-Cycle Fatigue Life of Type 321 Stainless Steel", *Journal of the Iron and Steel Institute of Japan*, Vol 64, No. 8 (July 1978), pp 1199–1208.

71 Luther, R. G., and Williams, T.R.G., "Fatigue Cycling of an Austenitic Stainless Steel in R = -1 Loadings", *Metal Science*, Vol 14, No. 1 (January 1980), pp 29–33.

72 Koster, W. P., Field, M., and Fritz, L. J., "Low Stress Creep Testing of 321 Stainless Steel", Research Report, Contract AF 33(600)-36430 (April 22, 1959).

73 Yoshida, S., Kanazawa, K., Yamaguchi, K., Sato, M., and Kobayashi, K., "Elevated-Temperature Fatigue Properties of Engineering Materials, Part II – Section 4: Elevated-Temperature Fatigue Properties of 18Cr-10Ni-Ti Stainless Steel Bars for General Application (SUS 321-B)", *Transactions of the National Research Institute for Metals*, Vol 20, No. 1 (January 1978), pp 60–73.

74 Yamaguchi, K., and Kanazawa, K., "Influence of Thermal Aging on High Temperature, Low-Cycle Fatigue Life of SUS 321 Stainless Steel", *Transactions of the National Research Institute for Metals*, Vol 25, No. 3 (September 1983), pp 143–147.

75 Yamaguchi, K., Kanazawa, K., and Yoshida, S., "Some Aspects of Cracks in Austenitic Stainless Steels Low-Cycle Fatigued at High Temperatures", *Transactions of the National Research Institute for Metals*, Vol 18, No. 4 (July 1976), pp 128–132.

76 Yamaguchi, K., and Kanazawa, K., "Influence of Grain Size on the Low-Cycle Fatigue Lives of Austenitic Stainless Steels at High Temperatures", *Metallurgical Transactions*, Vol 11A, No. 10 (October 1980), pp 1691–1699.

77 Michel, D. J., and Smith, H. H., "Effect of Hold Time and Thermal Aging on Elevated Temperature Fatigue Crack Propagation in Austenitic Stainless Steels", Naval Research Laboratory Report NRL-MR-3627 (October 1977).

78 Yamaguchi, K., and Kanazawa, K., "Crack Propagation Rates of Austenitic Stainless Steels Under High-Temperature Low-Cycle Fatigue Conditions", *Metallurgical Transactions*, Vol 10A, No. 10 (October 1979), pp 1445–1451.

79 Gupta, A. K., Hughes, K. E., and Sellars, C. M., "Glass-Lubricated Hot Extrusion of Stainless Steel", *Metals Technology*, Vol 7, No. 8 (August 1980), pp 323–331.

80 Daly, J. J., "Weldments Live Longer With Shot-Peening", *Welding Design and Fabrication*, Vol 50, No. 7 (July 1977), pp 74–76.

81 Iwami, J-I., Kishimoto, K., and Yamaguchi, A., "Solidification Crack Susceptibility in the Weld Metals of Austenitic Stainless Steels and Ni-Base Super Alloys", *Transactions of the Iron and Steel Institute of Japan*, Vol 23, No. 6 (June 1983), p B-217.

82 Whittle, R.D.T., and Scott, V. D., "Sliding-Wear Evaluation of Nitrided Austenitic Alloys", *Metals Technolgoy*, Vol 11, No. 6 (June 1984), pp 231–241.

83 Whittle, R.D.T., and Scott, V. D., "Sliding-Wear Evaluation of Boronized Austenitic Alloys", *Metals Technology*, Vol 11, No. 12 (December 1984), pp 522–529.

84 Knotek, O., Lugschieder, E., and Reimann, H., "Wear-Resistant and Corrosion-Resistant Nickel-Base Alloys for Coating by Furnace Melting", *Thin Solid Films*, Vol 64, No. 3 (December 17, 1979), pp 365–369.

85 "AISI Type 321", Alloy Digest, Filing Code: SS-124 (November 1961).

Alloy	Type 321
AMS Specification	Product Form
5645L	Bars, Forgings
5510M	Sheet, Strip, Plate
5689C	Wire
5576G	Tubing, Welded
5559E	Tubing, Welded, Thin Wall
5570L	Tubing, Seamless
5557F	Tubing, Seamless and Welded, Hydraulic

Fe
18 Cr
10 Ni
+ Ti

Type 321

TABLE 1.031. SPECIFICATIONS (1–7)

Alloy	Type 321											
AMS Specification	5645L		5689C		5510M, 5559E		5576G		5570L		5557F	
	Percent											
Element	Min	Max	Min	Max	Min	Max	Min	Max	Min	Max	Min	Max
Chromium	17.00	19.00	17.00	19.00	17.00	19.00	17.00	19.00	17.00	19.00	17.00	20.00
Nickel	8.00	12.00	8.00	11.00	9.00	12.00	9.00	12.00	9.00	13.00	8.00	13.00
Titanium	5x(C+N)	0.70	5x(C+N)	0.70	5x(C+N)	0.70	5x(C+N)	0.70	5x(C+N)	0.70	5x(C+N)	0.70
Carbon	–	0.08	–	0.08	–	0.08	–	0.08	–	0.08	–	0.08
Manganese	–	2.00	–	2.00	–	2.00	–	2.00	–	2.00	–	2.00
Silicon	–	1.00	–	1.00	0.40	1.00	–	1.00	0.40	1.00	0.40	1.00
Copper	–	0.75	–	0.75	–	0.75	–	0.75	–	0.75	–	0.75
Molybdenum	–	0.75	–	0.75	–	0.75	–	0.75	–	0.75	–	0.75
Nitrogen	–	0.10	–	0.10	–	0.10	–	0.10	–	0.10	–	0.10
Phosphorus	–	0.040	–	0.040	–	0.040	–	0.040	–	0.040	–	0.040
Sulfur	–	0.030	–	0.030	–	0.030	–	0.030	–	0.030	–	0.030

TABLE 1.041. COMPOSITION (1–7)

Alloy	Type 321
Condition	Annealed
Form	Hardness
Bars, Plates	150–228 BHN
Tube, Sheet, Strip	80–95 HRB
Wire	95 HRB

TABLE 1.061. HARDNESS OF VARIOUS FORMS (8,9,10,31)

Alloy	Type 321	
Condition	Annealed	
Exposure Time, hr	1000	10,000
Exposure Temperature, F	BHN	
Unexposed	168	168
900	143	156
1050	149	151
1200	166	148

TABLE 1.062. EFFECTS OF EXPOSURES TO ELEVATED TEMPERATURES ON HARDNESS AT ROOM TEMPERATURE (11)

Fe
18 Cr
10 Ni
+ Ti

Type 321

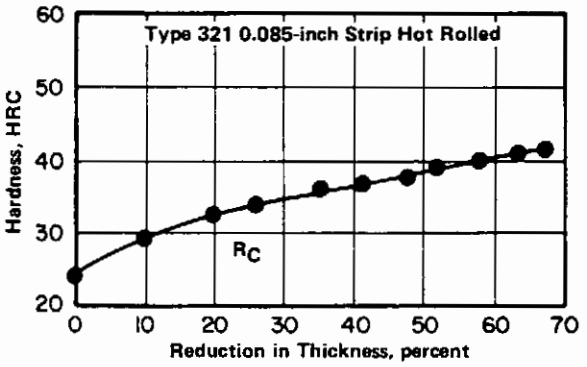

FIGURE 1.063. EFFECT OF COLD ROLLING ON HARDNESS OF STRIP (21)

Alloy	Type 321
Forms	Conditions
Forgings	Annealed
Billets	Annealed
Bars	Hot Rolled or Cold Drawn
Sheet and Strip	Annealed or Temper Rolled up to 1/2 Hard
Wire	Annealed or Cold Drawn to Specified Temper
Wire Rod	Annealed
Plates	Annealed

TABLE 1.07. FORMS AND CONDITIONS AVAILABLE (9,10,33)

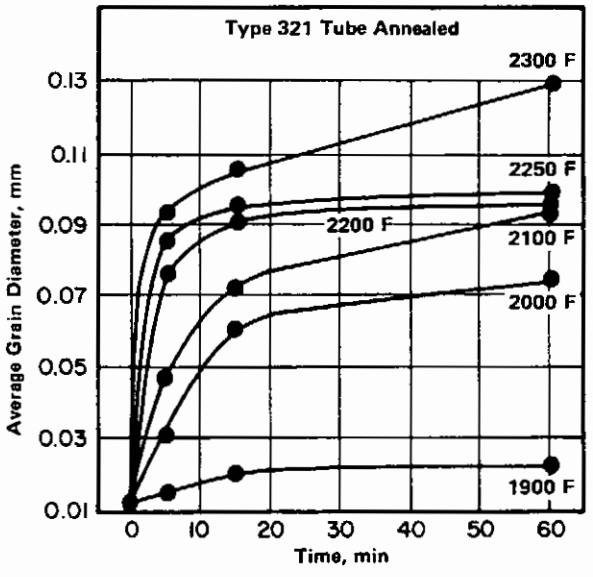

FIGURE 1.0921. EFFECTS OF TIME AND TEMPERATURE ON GRAIN GROWTH (15)

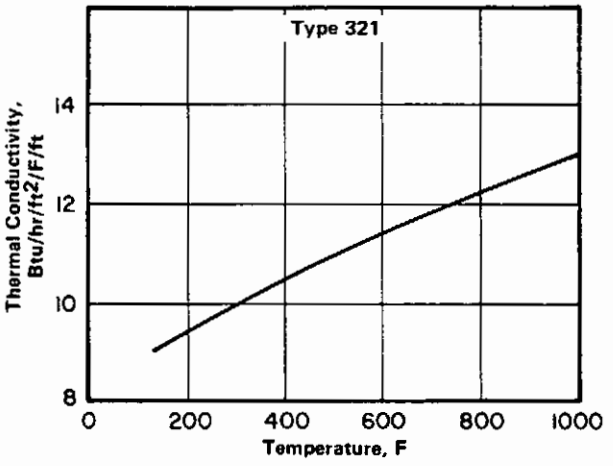

FIGURE 2.013. THERMAL CONDUCTIVITY (34)

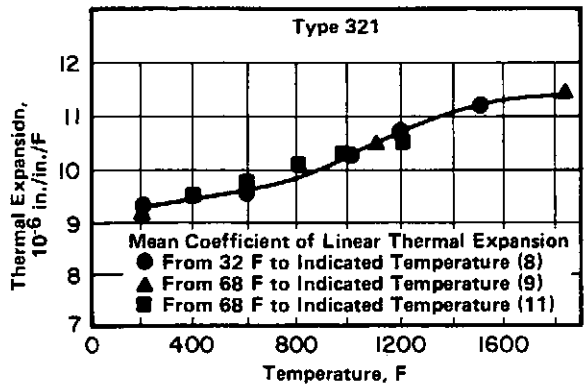

FIGURE 2.014. THERMAL EXPANSION (8,9,11)

Alloy	Type 321		
Condition	Annealed		
	Electrical Conductivity		Electrical Resistivity, μΩ-in.
Temperature, F	Percent IACS	Mmhos/in.^{3}	
68	2.41	0.0354	28.3
212	2.22	0.0326	30.7
392	2.01	0.0296	33.8
752	1.73	0.0254	39.4
1112	1.56	0.0229	43.7
1472	1.43	0.0210	47.6
1652	1.37	0.0202	49.6

TABLE 2.0221. ELECTRICAL PROPERTIES AT VARIOUS TEMPERATURES (9)

Fe
18 Cr
10 Ni
+ Ti

Type 321

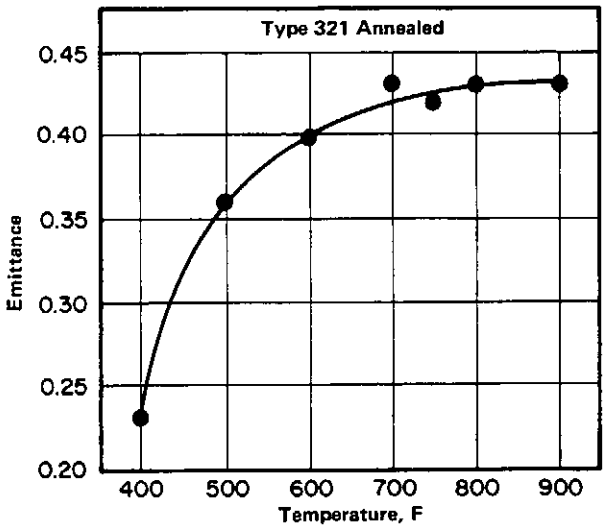

FIGURE 2.0241. TOTAL NORMAL EMITTANCE AT ELEVATED TEMPERATURES (24)

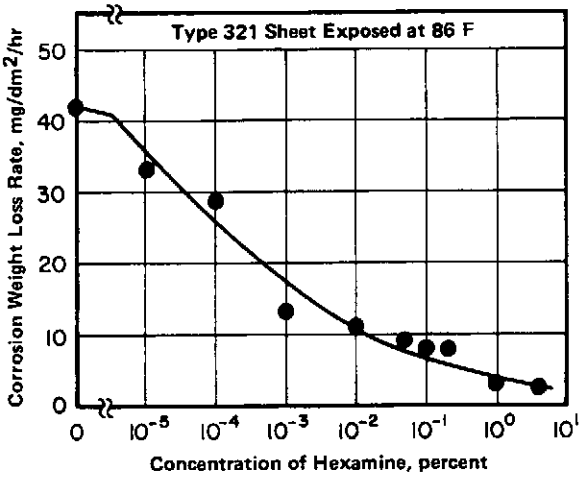

FIGURE 2.0315. EFFECTS OF HEXAMINE ON CORROSION OF TYPE 321 IN 1N HCl (51)

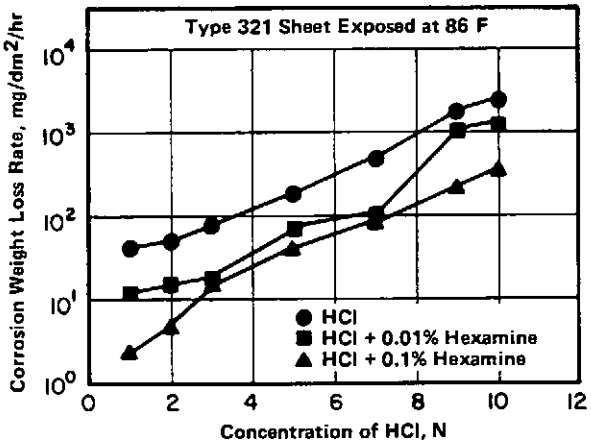

FIGURE 2.0316. EFFECTS OF HYDROCHLORIC ACID CONCENTRATION AND HEXAMINE ON CORROSION OF TYPE 321 (51)

Fe
18 Cr
10 Ni
+ Ti

Type 321

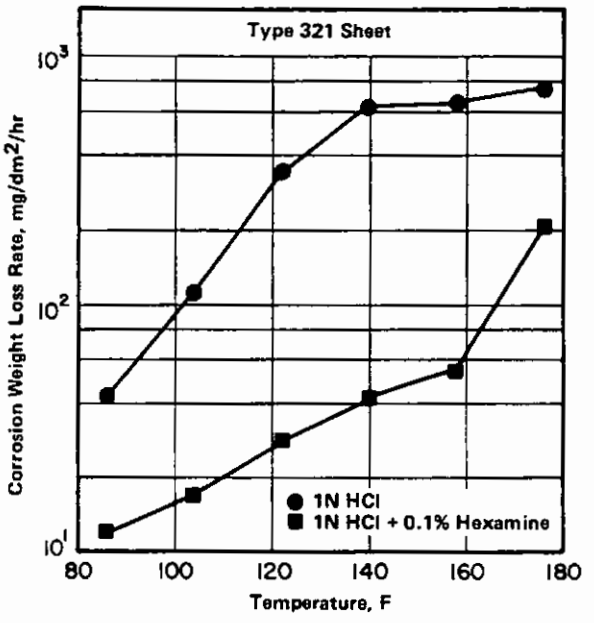

FIGURE 2.0317. EFFECTS OF TEMPERATURE AND HEXAMINE ON CORROSION OF TYPE 321 IN HYDROCHLORIC ACID (51)

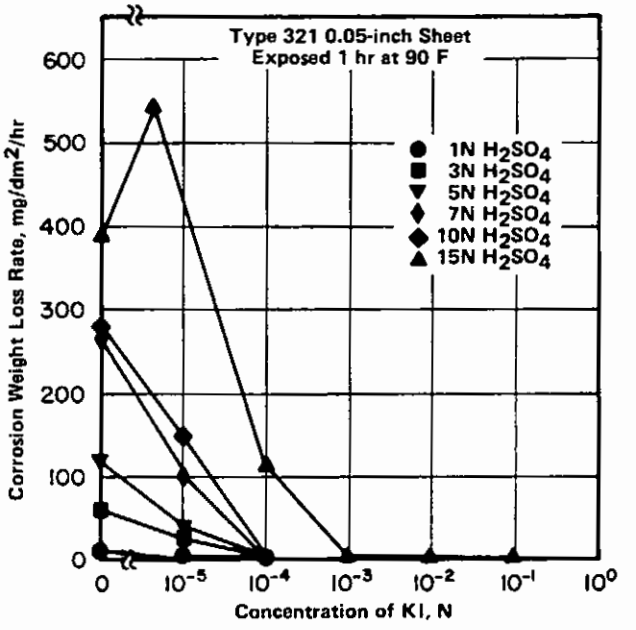

FIGURE 2.0319. EFFECTS OF POTASSIUM IODIDE ON SULFURIC ACID CORROSION OF TYPE 321 (52)

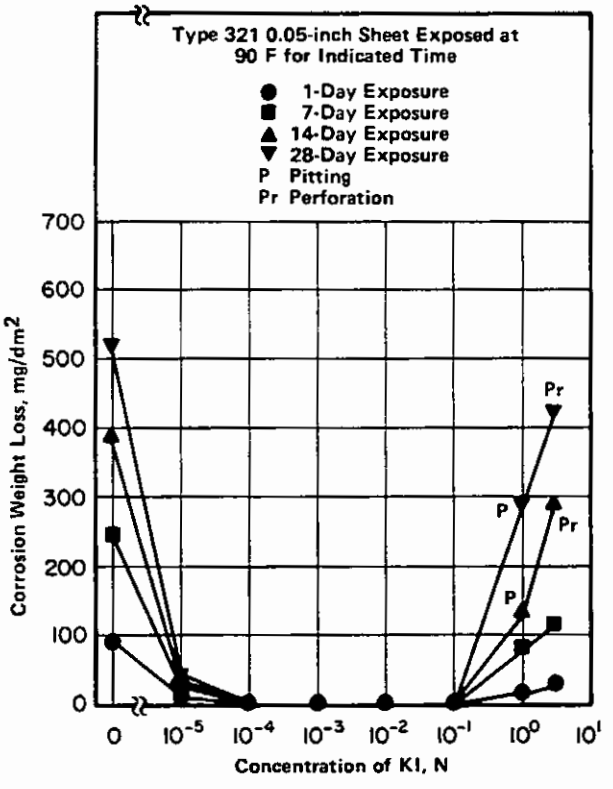

FIGURE 2.03110. EFFECTS OF POTASSIUM IODIDE AND EXPOSURE TIME ON CORROSION WEIGHT LOSS IN 1N SULFURIC ACID (52)

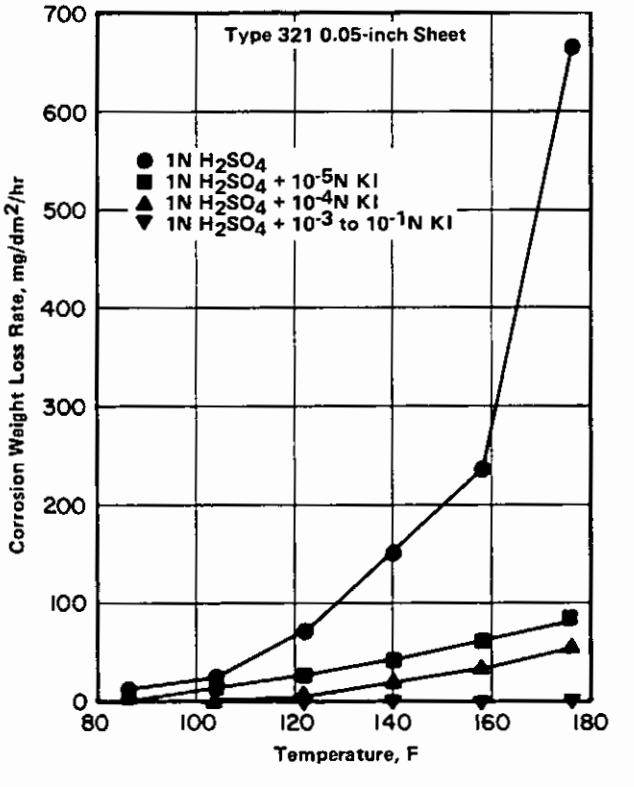

FIGURE 2.03111. EFFECT OF TEMPERATURE AND POTASSIUM IODIDE ON CORROSION OF TYPE 321 IN SULFURIC ACID (52)

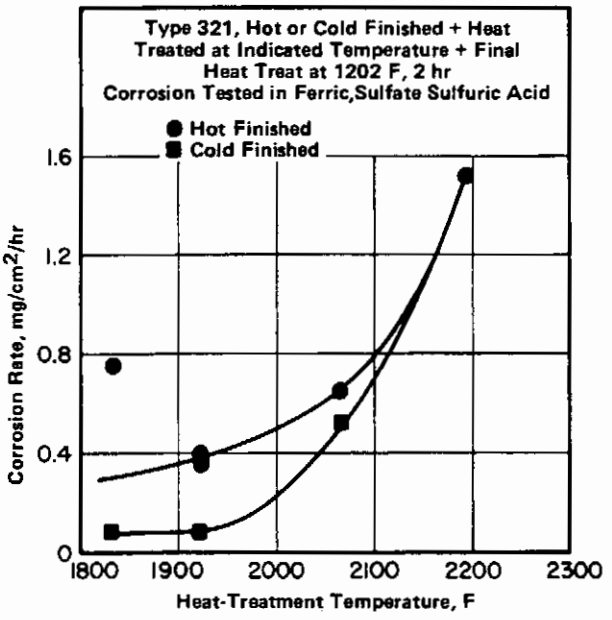

FIGURE 2.0322. EFFECTS OF HIGH-TEMPERATURE HEAT TREATMENT ON CORROSION RATE OF TYPE 321 (53)

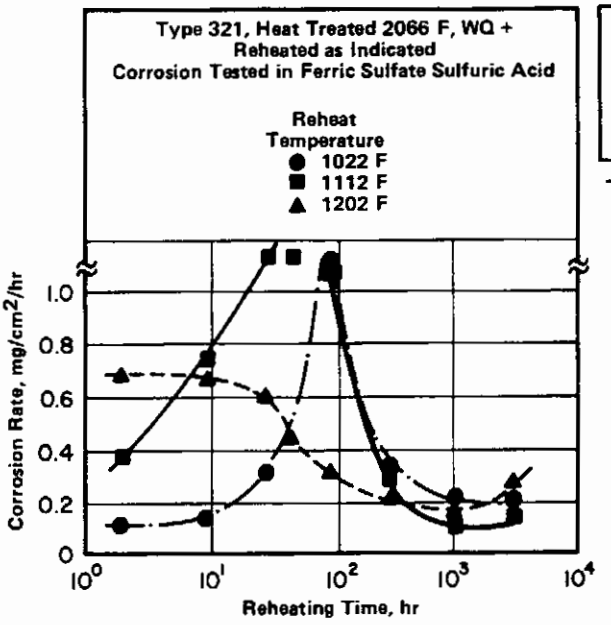

FIGURE 2.0323. EFFECTS OF SENSITIZATION REHEATING ON CORROSION RATES OF SOLUTION-ANNEALED TYPE 321 (53)

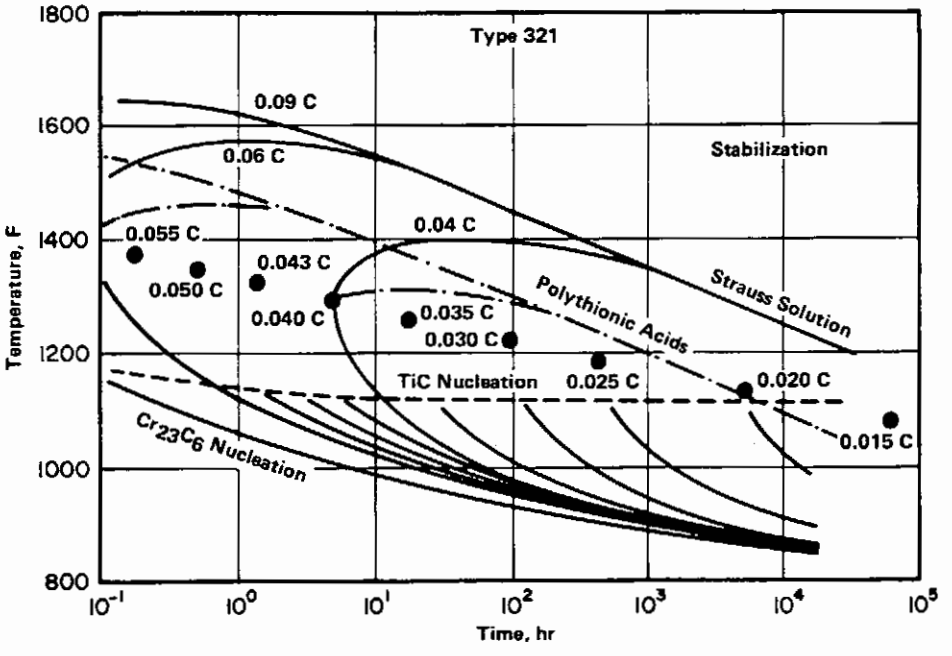

FIGURE 2.0324. TIME-TEMPERATURE-DISSOLVED CARBON RELATIONSHIPS FOR $Cr_{23}C_6$ PRECIPITATION AND FOR STABILIZATION IN 18Cr-8Ni TYPE STAINLESS STEELS (53)

Fe
18 Cr
10 Ni
+ Ti

Type 321

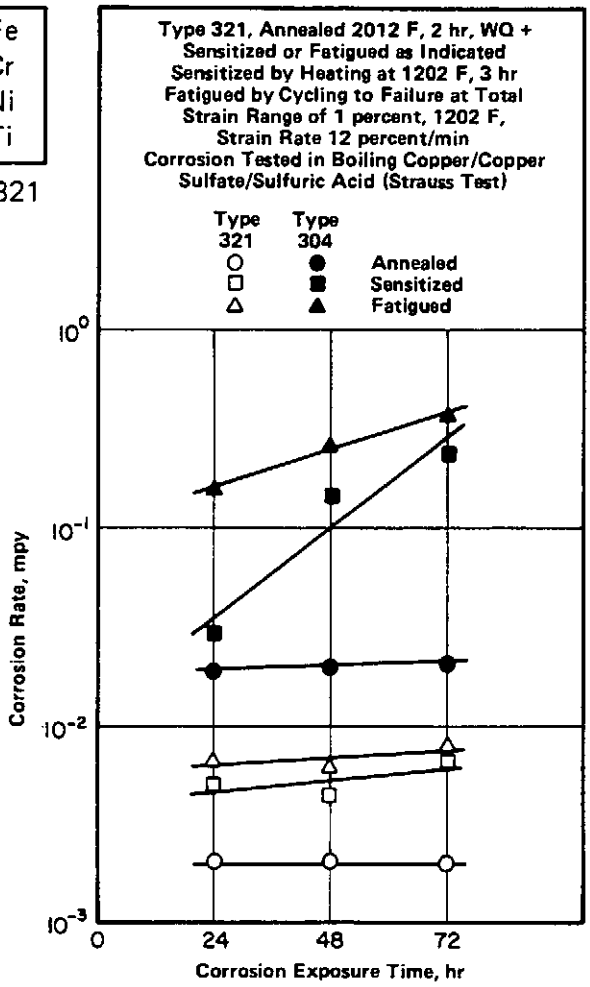

FIGURE 2.0326. EFFECTS OF SENSITIZING HEAT TREATMENT AND FATIGUE CYCLING ON CORROSION BEHAVIOR IN BOILING COPPER SULFATE (55)

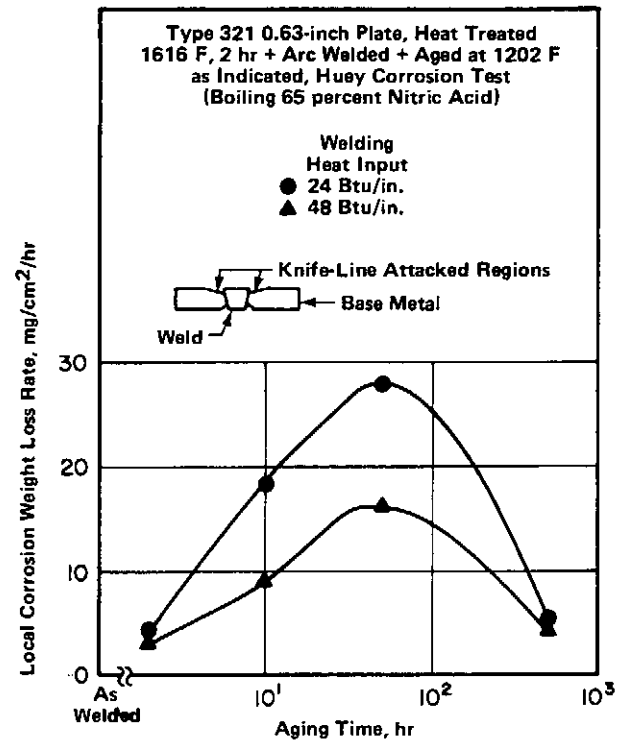

FIGURE 2.0328. EFFECTS OF AGING TIME ON KNIFE-LINE CORROSION RATE OF ARC-WELDED ALLOY (56)

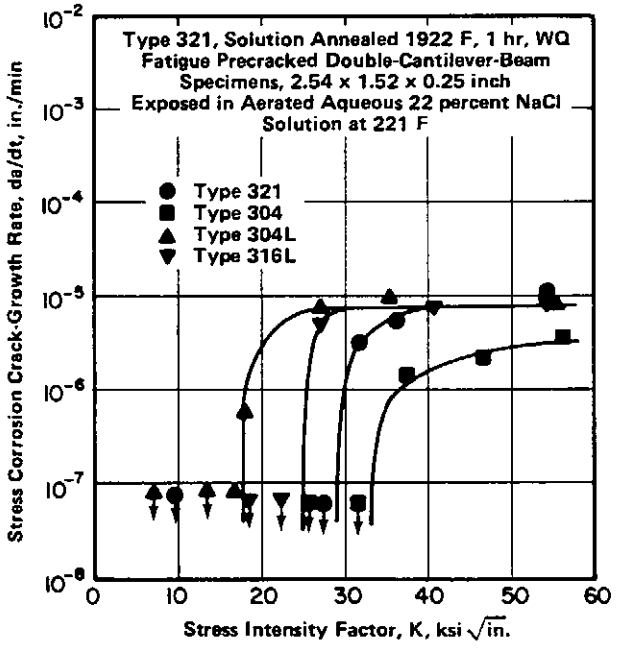

FIGURE 2.0333. EFFECT OF STRESS-INTENSITY FACTOR ON STRESS-CORROSION CRACK-GROWTH RATE IN HOT NaCl SOLUTION FOR TYPE 321 AND THREE OTHER AUSTENITIC STAINLESS STEELS (62)

Fe
18 Cr
10 Ni
+ Ti

Type 321

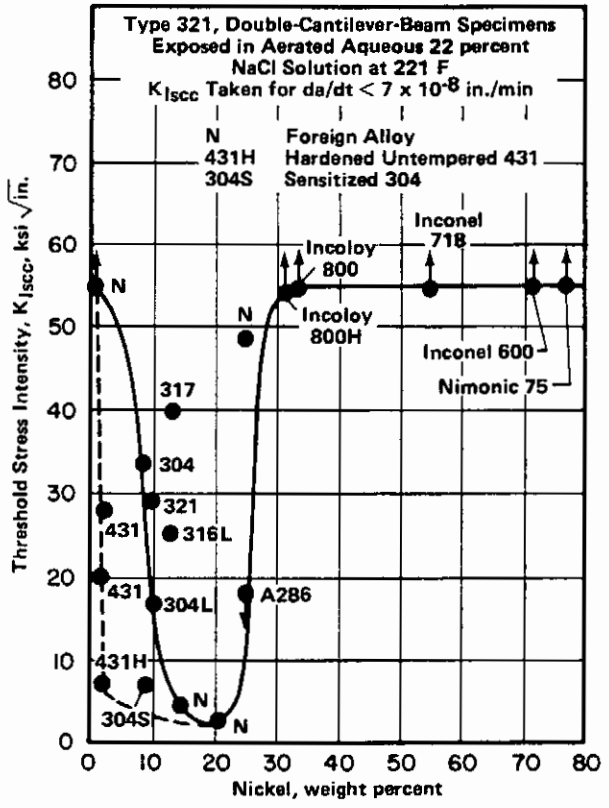

FIGURE 2.0334. EFFECT OF NICKEL CONTENT ON THRESHOLD STRESS INTENSITY FOR CORROSION CRACKING IN HOT NaCl SOLUTION FOR IRON-NICKEL ALLOYS CONTAINING ABOUT 18 PERCENT CHROMIUM (62)

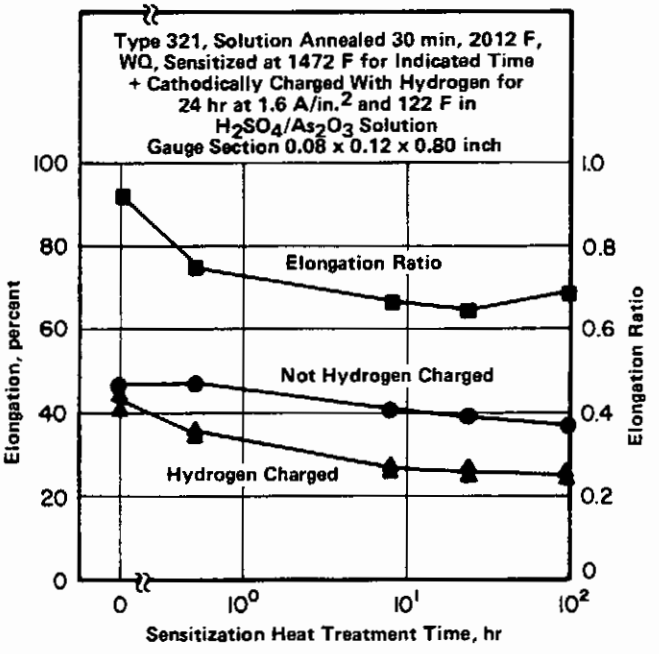

FIGURE 2.0342. EFFECTS OF HYDROGEN CHARGING AND SENSITIZATION ON TENSILE DUCTILITY AT -321 F (63)

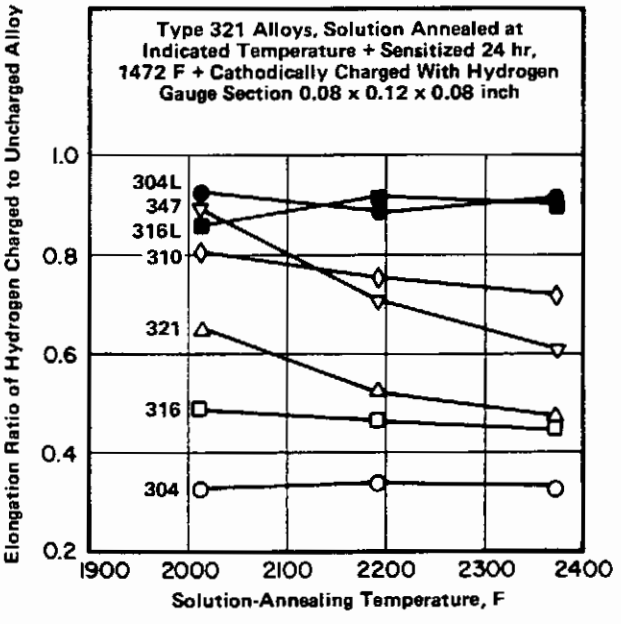

FIGURE 2.0343. EFFECTS OF SOLUTION-ANNEALING TEMPERATURE ON ELONGATION RATIO AT -321 F FOR TYPE 321 AND SIX OTHER AUSTENITIC STAINLESS STEELS (63)

Fe
18 Cr
10 Ni
+ Ti

Type 321

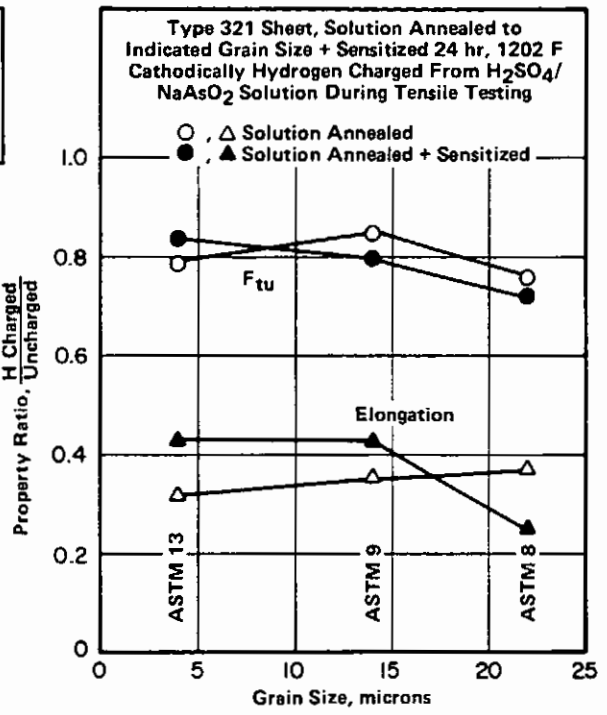

FIGURE 2.0345. EFFECTS OF GRAIN SIZE AND HEAT TREATMENT ON HYDROGEN EMBRITTLEMENT DURING TENSILE TESTING AT ROOM TEMPERATURE (64)

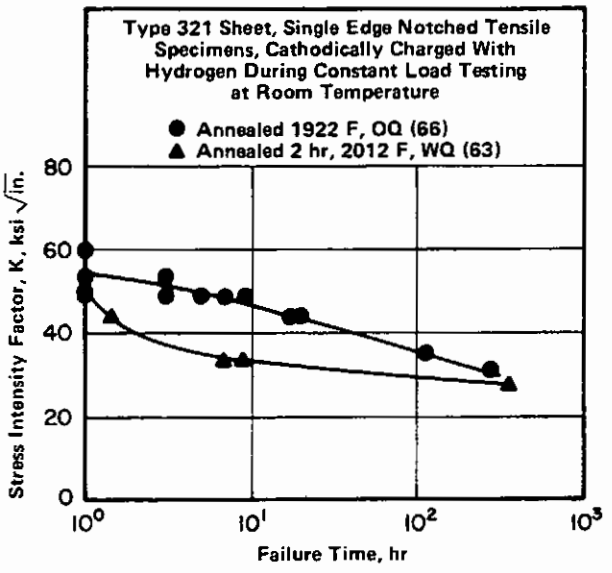

FIGURE 2.0347. EFFECTS OF HYDROGEN CHARGING ON DELAYED FAILURE BEHAVIOR OF TYPE 321 (65,66)

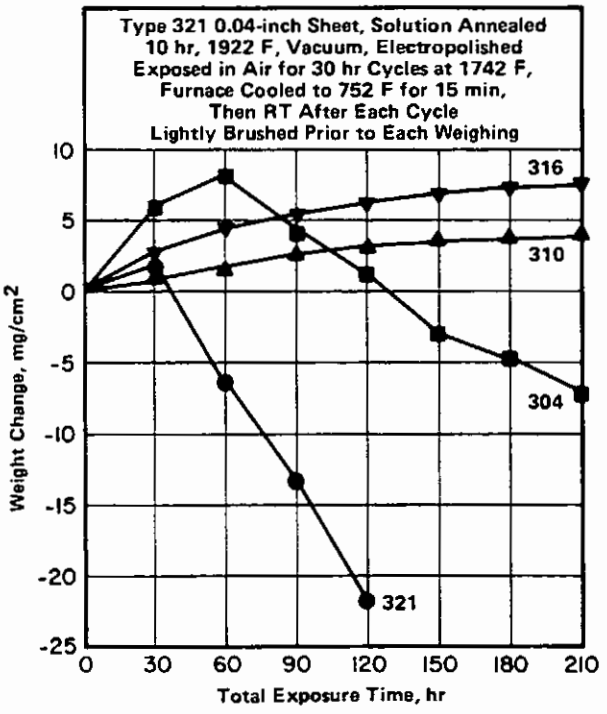

FIGURE 2.0352. OXIDATION WEIGHT-CHANGE BEHAVIOR OF TYPE 321 IN AIR AT 1742 F AS COMPARED TO TYPES 304 310, AND 316 (68)

Fe
18 Cr
10 Ni
+ Ti

Type 321

Alloy	Type 321				
Form	Tubing				
Condition Prior to Neutron Exposure	Test Temp., F	Neutron Fluence at 1000 to 1300 F, nvt (E > 1 MeV)	F_{ty}, ksi	F_{tu}, ksi	e (1 in.), percent
Annealed	75	Unexposed	34.4	79.0	59
	1100	Unexposed	35.6	51.5	28
	1300	Unexposed	26.5	32.2	31
	1500	Unexposed	13.2	16.2	32
Annealed	1100	6.7×10^{21}	60.9	65.5	3.8
	1300	1.3×10^{21}	34.1	36.0	7.8
	1300	6.7×10^{21}	35.9	37.3	2.0
Ann. + Exposed 24 hr at 1650 F	1100	2.5×10^{21}	57.6	60.0	2.8
	1300	0.76×10^{21}	24.5	29.6	15.0
	1300	3.0×10^{21}	29.6	32.0	5.6
	1500	2.4×10^{21}	14.2	15.4	10.0

TABLE 2.042. EFFECTS OF FAST-NEUTRON IRRADIATION ON TENSILE PROPERTIES AT ELEVATED TEMPERATURES (23)

Alloy	Type 321							
AMS Spec.	Product Form[a]	Thickness, in.	F_{ty}, ksi, Min	F_{tu}, ksi		El., percent, Min	Hardness, BHN	
				Min	Max		Min	Max
5559E	Tubing	–	35	75	105	40[b]	–	–
5576G, 5570L	Tubing	Up to 0.188 in. OD						
		Up to 0.016 in. Wall	–	–	120	33	–	–
		Over 0.016 in. Wall	–	–	105	35	–	–
		Over 0.188 to 0.500 in. OD						
		Up to 0.010 in. Wall	–	–	115	35[b]	–	–
		Over 0.010 in. Wall	–	–	105	35[b]	–	–
		Over 0.500 in. OD						
		Up to 0.010 in. Wall	–	–	120	30[b]	–	–
		Over 0.010 in. Wall	–	–	105	35[b]	–	–
5557F	Tubing	Up to 0.188 in. OD						
		Up to 0.016 in. Wall	30	75	120	33	–	–
		Over 0.016 in. Wall	30	75	105	35	–	–
		Over 0.188 to 0.500 in. OD						
		Up to 0.010 in. Wall	30	75	115	35[b]	–	–
		Over 0.010 in. Wall	30	75	105	35[b]	–	–
		Over 0.500 in. OD						
		Over 0.010 in. Wall	30	75	105	35[b]	–	–
5510M	Sheet, Strip, Plate	>0.002–0.003	–	–	110	20	–	–
		>0.003–0.004	–	–	105	30	–	–
		>0.004	–	–	100	40	–	–
5645L	Wire[c]	–	–	85	125	–	–	–
	Bars	Up to 2.00	–	–	–	–	140	255
		Over 2.00	–	–	–	–	–	255
	Forgings, Rings	–	–	–	–	–	–	187
5689C	Wire[c]	0.010–0.020	–	–	135	–	–	–
		>0.020–0.125	–	–	125	–	–	–
		>0.125–0.250	–	–	115	–	–	–

Note: The original AMS documents should be consulted for complete specification details.
(a) All materials in solution-heat-treated condition.
(b) Tube elongation values pertain to full tube; strip specimens 5 percent lower.
(c) Wire F_{tu} values pertain to straight lengths; coil specimens 10 ksi lower.

TABLE 3.011. AMS SPECIFIED MECHANICAL PROPERTIES

Fe
18 Cr
10 Ni
+ Ti

Type 321

Alloy	Type 321		
Condition	Annealed		
Form	F_{ty}, ksi	F_{tu}, ksi	e (2 in.), percent
Bar	35	85	55
Plate	30	85	55
Sheet	35	90	45
Strip	35	90	45
Tubing	35	85	50
Wire	65	95	40

TABLE 3.0212. TENSILE PROPERTIES OF VARIOUS FORMS (31)

Alloy	Type 321			
Condition	Annealed			
100,000-hr Exposure Temp, F	F_{ty}, ksi	F_{tu}, ksi	e (2 in.), percent	RA, percent
Unexposed	30.0	77.3	61	81
900	45.6	84.7	51	81
1050	32.2	86.6	48	70
1200	25.8	82.1	48	62

TABLE 3.0213. EFFECTS OF 100,000-HOUR EXPOSURE TO ELEVATED TEMPERATURES ON ROOM-TEMPERATURE TENSILE PROPERTIES (11)

Alloy	Type 321					
Condition	Annealed at 1900 F					
Form	1-inch-Dia Bar					
Exposure Temp, F	Exposure Load, ksi	Exposure Time, hr	F_{ty}, ksi	F_{tu}, ksi	e (2 in.), percent	RA, percent
70	–	–	67.0	93.0	49	75
1100	12.5	1679	61.0	96.5	48	70
1200	7.0	1367	59.7	96.3	42	56
1300	5.0	1656	54.5	96.5	39	52

TABLE 3.0214. EFFECTS ON ROOM-TEMPERATURE TENSILE PROPERTIES OF ELEVATED-TEMPERATURE EXPOSURES UNDER LOAD (35)

Alloy	Type 321				
Form	0.75 inch x 3-1/8 inch Extruded Flat				
Condition	Orientation	F_{ty}, ksi	F_{tu}, ksi	e (4D), percent	RA, percent
As Hot Extruded	L	20.8	67.2	62.5	75
	T	27.0	65.0	69	75
Ann. 1950 F, 1 hr, WQ	L	24.2	67.0	58	79
	T	22.5	64.4	67	75

TABLE 3.0215. TENSILE PROPERTIES OF EXTRUSIONS (14)

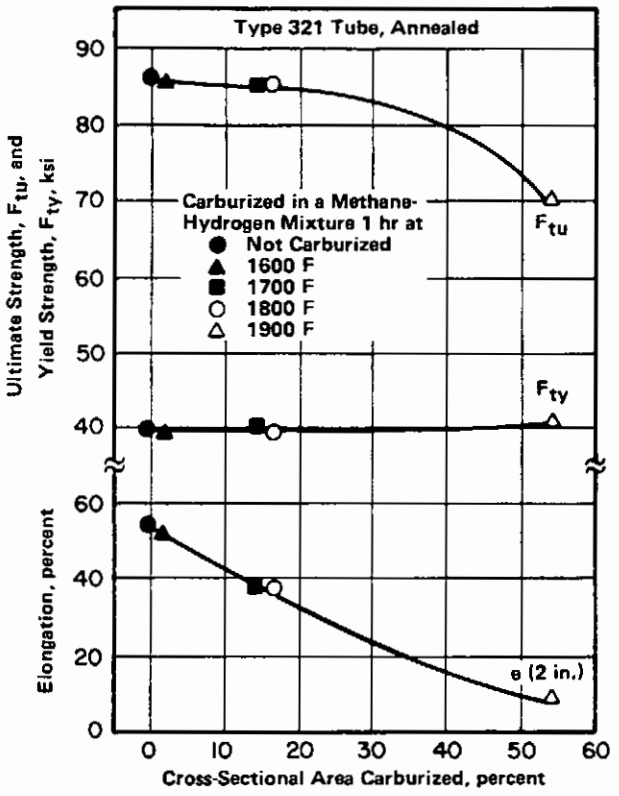

FIGURE 3.0216. EFFECT OF CARBURIZING ON ROOM-TEMPERATURE TENSILE PROPERTIES (16)

Alloy	Type 321	
Condition	Annealed	
Exposure Time, hr	1000	10,000
Exposure Temp, F	Charpy Keyhole, ft-lb	
Unexposed	107	107
900	101	88
1050	90	72
1200	69	62

Fe
18 Cr
10 Ni
+ Ti
Type 321

TABLE 3.0231. EFFECTS OF EXPOSURES TO ELEVATED TEMPERATURES ON ROOM-TEMPERATURE IMPACT PROPERTIES (11)

Alloy	Type 321		
Condition	Annealed at 1900 F		
Form	1-inch Dia Bar		
Exposure Temp, F	Exposure Load, ksi	Exposure Time, hr	Izod IE, ft-lb
70	–	–	92
1100	7.0	2750	54
1200	4.0	2753	49
1300	2.0	2612	46
1500	1.0	1601	41

TABLE 3.0232. EFFECTS ON ROOM-TEMPERATURE IMPACT PROPERTIES OF ELEVATED-TEMPERATURE EXPOSURES UNDER LOAD (35)

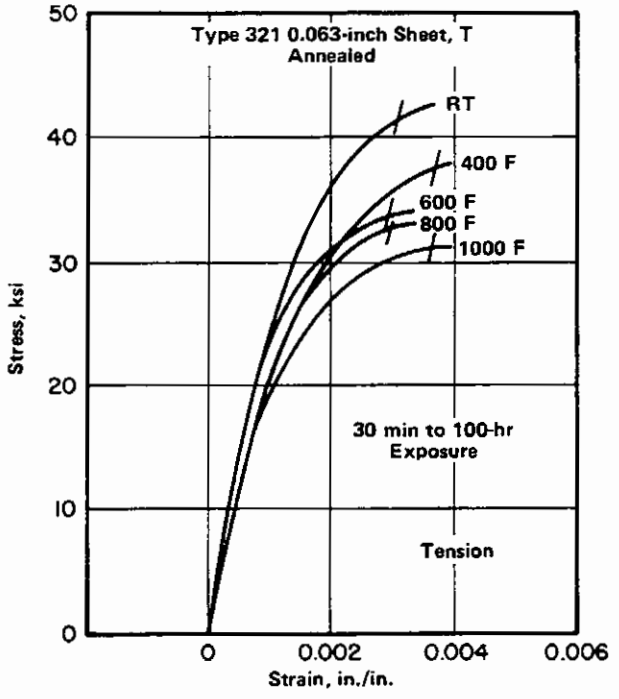

FIGURE 3.0311. STRESS-STRAIN CURVES FOR SHEET AT ROOM AND ELEVATED TEMPERATURES (36)

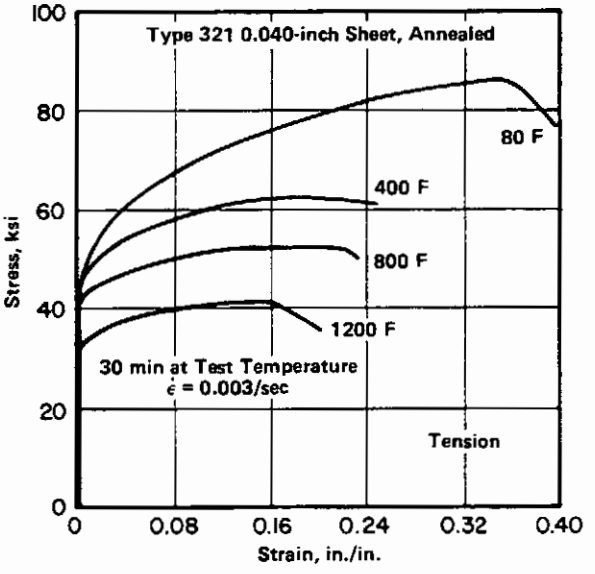

FIGURE 3.0312. COMPLETE STRESS-STRAIN CURVES FOR SHEET AT ROOM AND ELEVATED TEMPERATURES (37)

Fe
18 Cr
10 Ni
+ Ti

Type 321

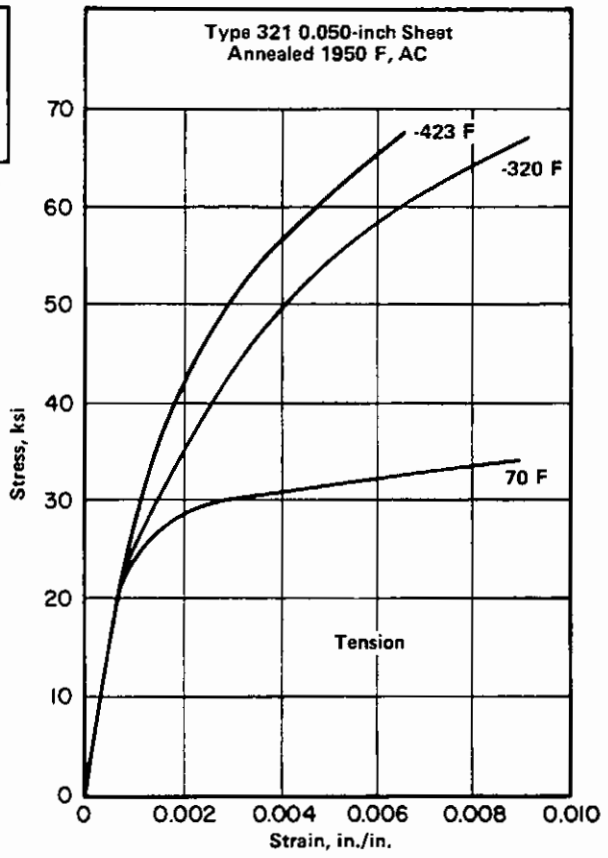

FIGURE 3.0313. STRESS-STRAIN CURVES FOR SHEET AT ROOM AND LOW TEMPERATURES (13)

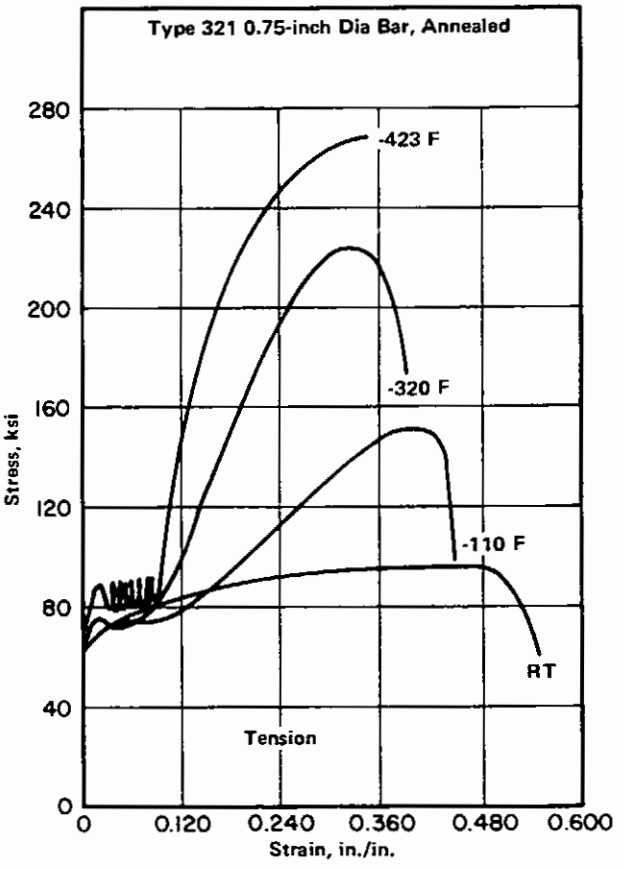

FIGURE 3.0314. COMPLETE STRESS-STRAIN CURVES FOR BAR AT ROOM AND LOW TEMPERATURES (38)

Fe
18 Cr
10 Ni
+ Ti

Type 321

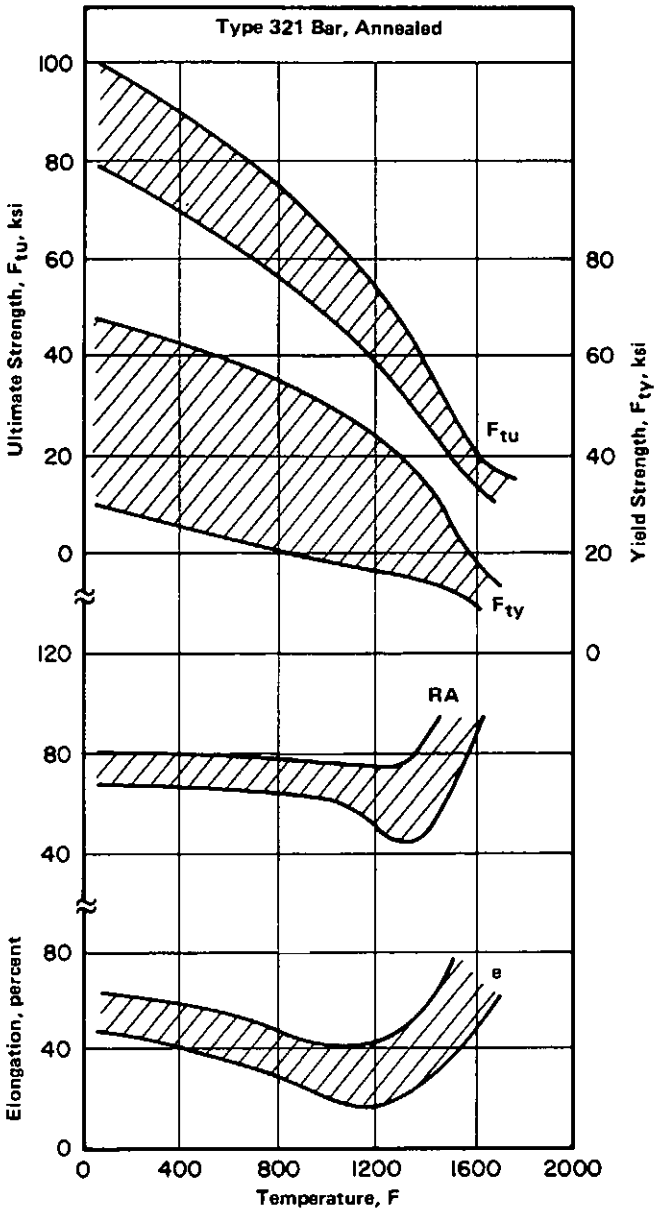

FIGURE 3.0315. SCATTER BANDS FOR TENSILE PROPERTIES OF BAR AT ROOM AND ELEVATED TEMPERATURES (39)

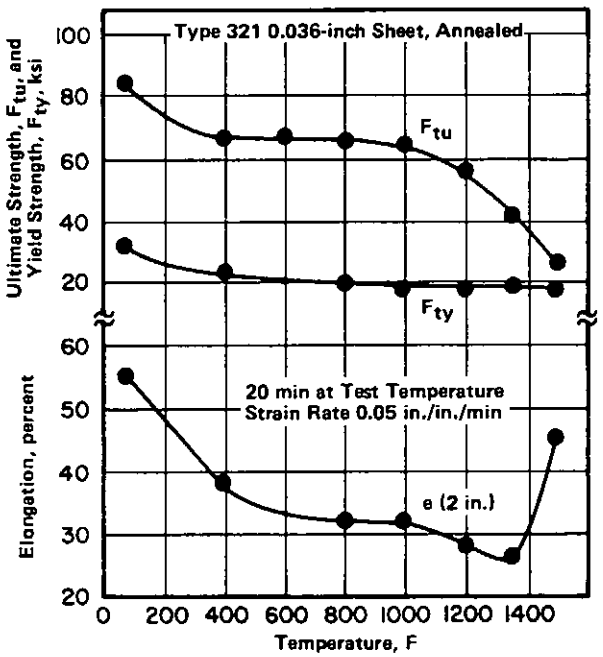

FIGURE 3.0316. EFFECT OF ELEVATED TEMPERATURES ON TENSILE PROPERTIES OF SHEET (9)

Fe
18 Cr
10 Ni
+ Ti

Type 321

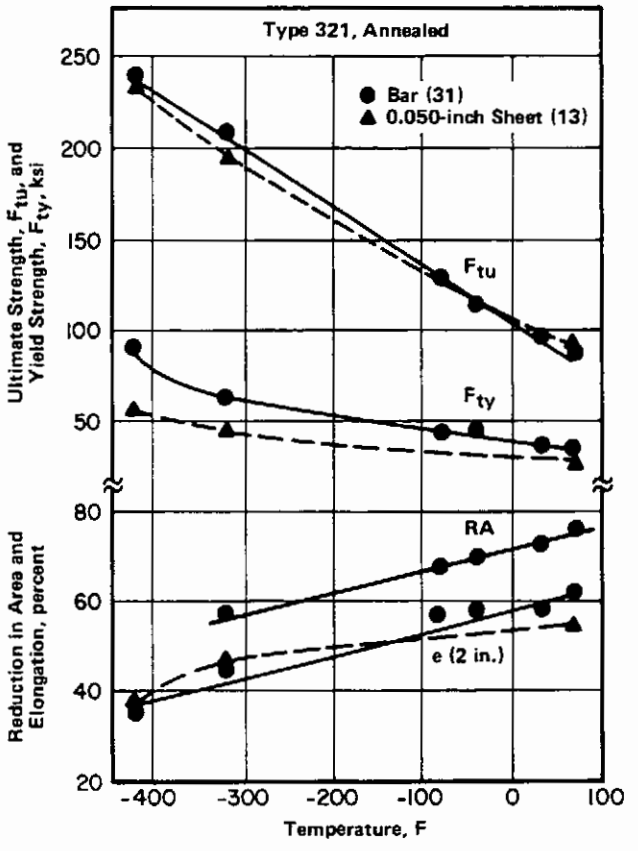

FIGURE 3.0317. EFFECTS OF LOW TEMPERATURES ON TENSILE PROPERTIES OF BAR AND SHEET (13,31)

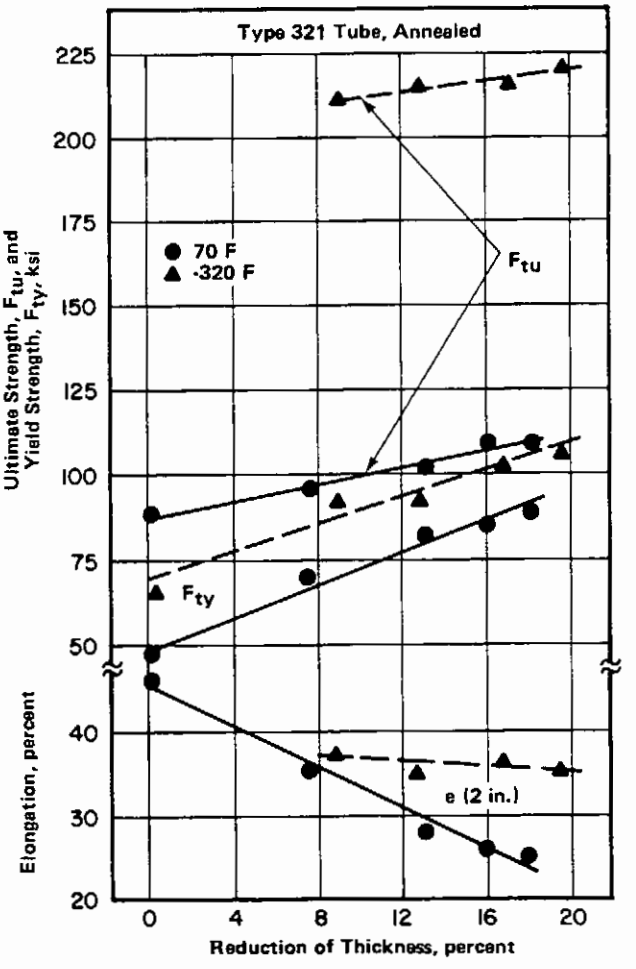

FIGURE 3.0318. EFFECTS OF COLD WORK INDUCED BY HYDRAULIC EXPANSION ON TENSILE PROPERTIES OF TUBING AT 70 F AND -320 F (19)

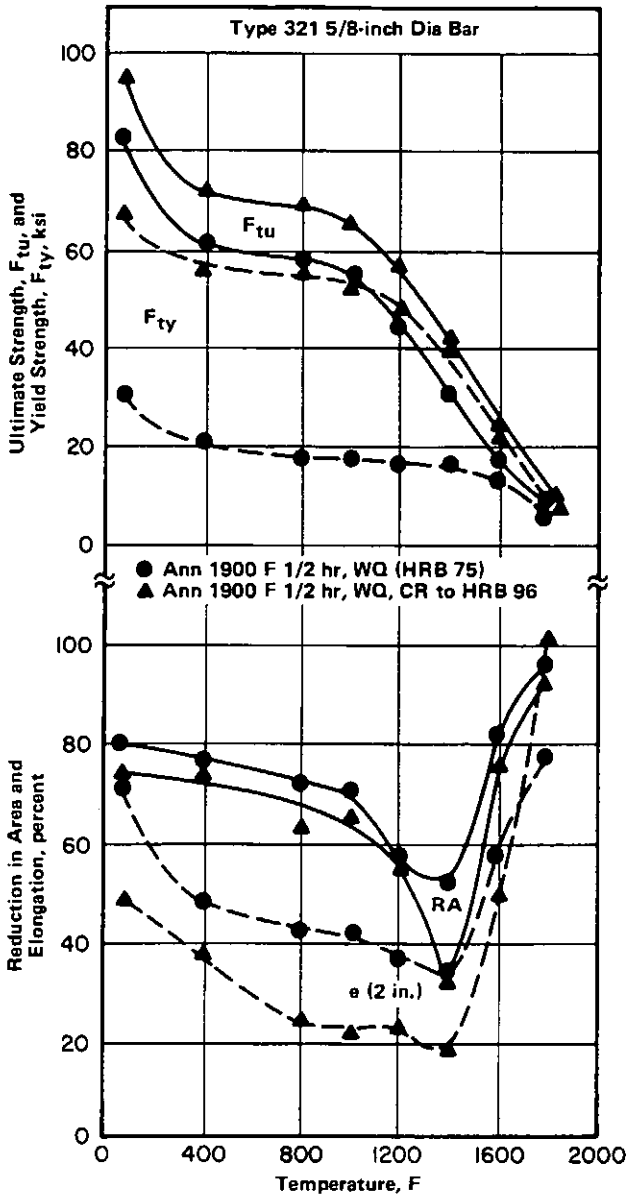

FIGURE 3.0319. EFFECTS OF TEMPERATURE ON TENSILE PROPERTIES OF ANNEALED AND COLD-ROLLED BAR (8)

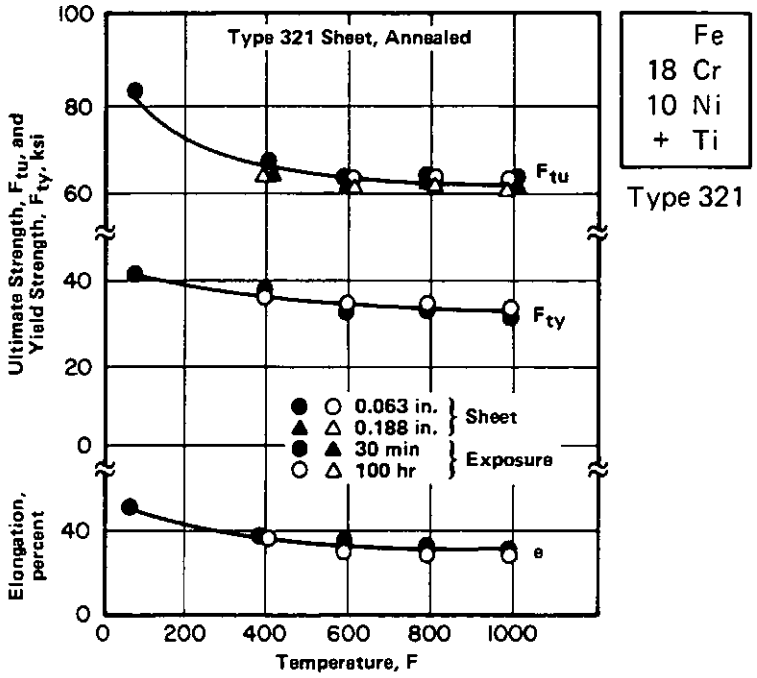

FIGURE 3.03110. EFFECTS OF TEST TEMPERATURE, AFTER TWO DIFFERENT EXPOSURE TIMES AT TEMPERATURE, ON TENSILE PROPERTIES OF SHEET (36)

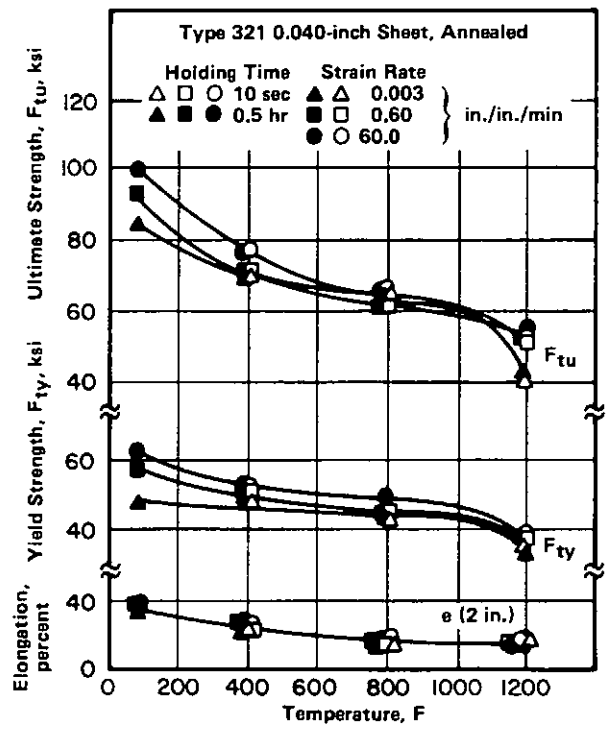

FIGURE 3.03111. EFFECTS OF TEMPERATURE, RAPID STRAIN RATES, AND SHORT HOLDING TIMES AT TEMPERATURE ON TENSILE PROPERTIES OF SHEET HEATED TO TEST TEMPERATURES WITHIN 10 SECONDS (40)

Fe
18 Cr
10 Ni
+ Ti

Type 321

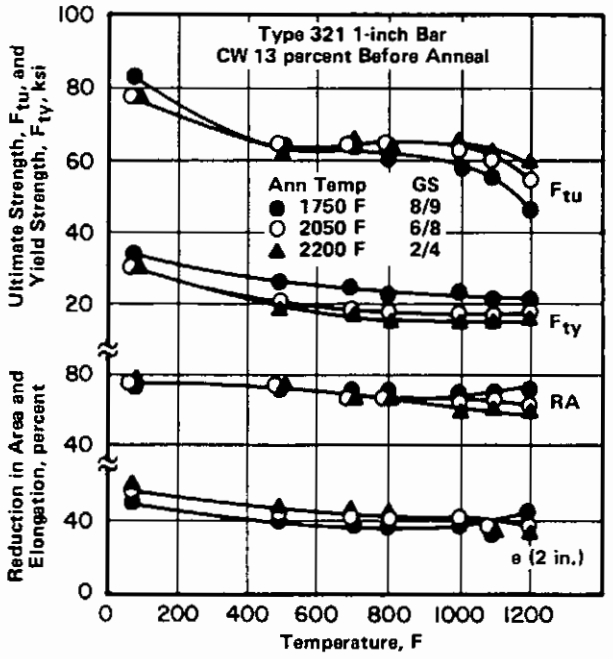

FIGURE 3.03112. EFFECTS OF TEMPERATURE ON TENSILE PROPERTIES OF BAR ANNEALED AT VARIOUS TEMPERATURES (35)

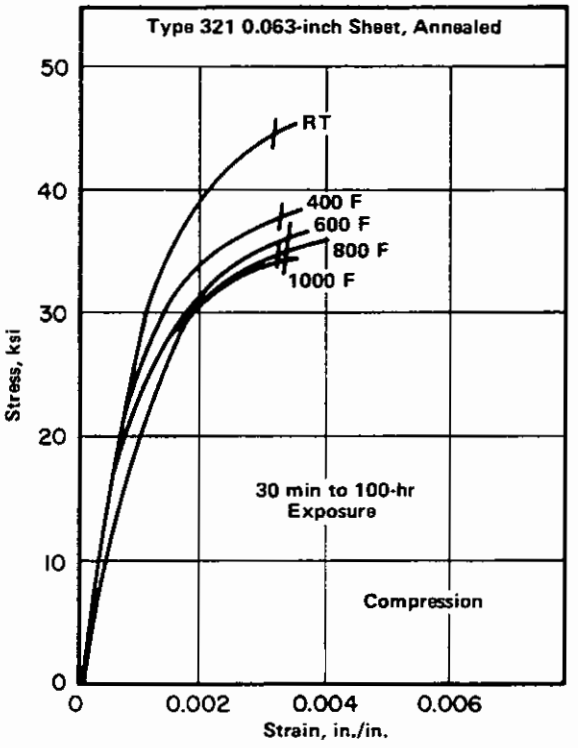

FIGURE 3.0321. COMPRESSIVE STRESS-STRAIN CURVES FOR SHEET AT ROOM AND ELEVATED TEMPERATURES (36)

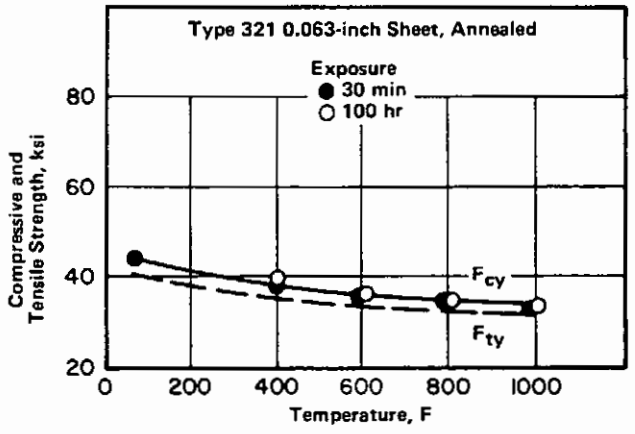

FIGURE 3.0322. EFFECTS OF TEMPERATURE, AFTER TWO DIFFERENT EXPOSURE TIMES AT TEMPERATURE, ON COMPRESSIVE YIELD STRENGTH OF SHEET (36)

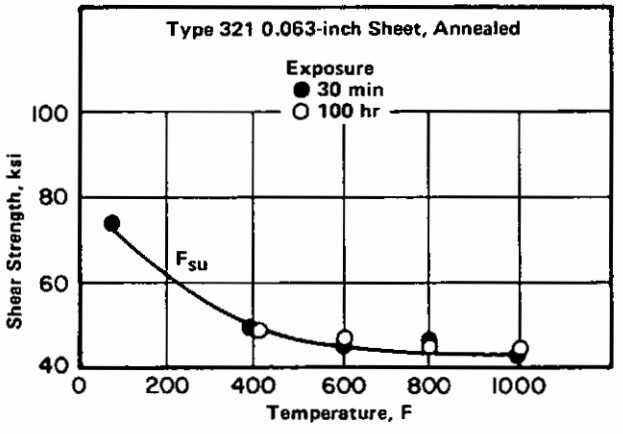

FIGURE 3.0351. EFFECTS OF TEMPERATURE, AFTER TWO DIFFERENT EXPOSURE TIMES AT TEMPERATURE, ON SHEAR STRENGTH OF SHEET (36)

Fe
18 Cr
10 Ni
+ Ti

Type 321

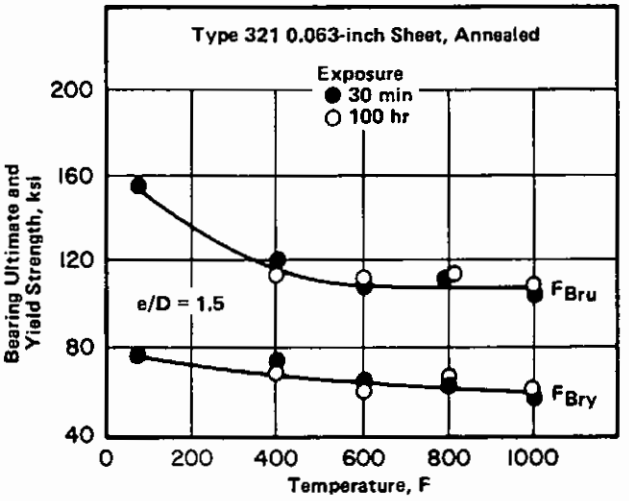

FIGURE 3.0361. EFFECTS OF TEMPERATURE, AFTER TWO DIFFERENT EXPOSURE TIMES AT TEMPERATURE, ON BEARING PROPERTIES OF SHEET (36)

Alloy	Type 321						
Condition	Annealed						
Form	Plate						
Temp, F	Specimen Type	Environment	Pressure, psig	F_{ty}, ksi	F_{tu}, ksi	e (4D), percent	RA, percent
70	Smooth	Air	0	32	87	77	71
70	Smooth	Helium	5000	29	84	63	66
70	Smooth	Hydrogen	5000	37	86	64	60
70	Notched	Helium	5000	–	113	–	6.4
70	Notched	Hydrogen	5000	–	99	–	2.3
-200	Smooth	Helium	5000	–	124	48	67
-200	Smooth	Hydrogen	5000	–	122	43	56
-200	Notched	Helium	5000	–	143	–	12
-200	Notched	Hydrogen	5000	–	141	–	12

Notched specimen

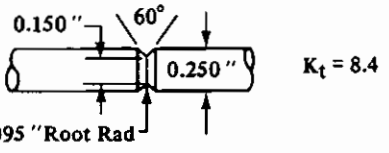

TABLE 3.03711. SMOOTH AND NOTCHED TENSILE PROPERTIES IN HIGH-PRESSURE HELIUM AND HYDROGEN AT 70 F AND -200 F

Fe
18 Cr
10 Ni
+ Ti

Type 321

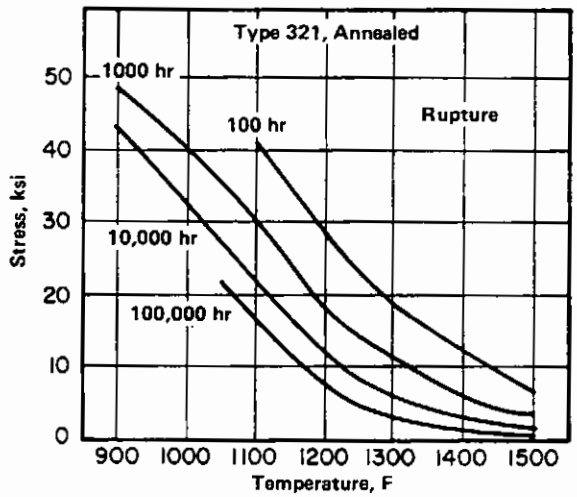

FIGURE 3.041. EFFECT OF TEMPERATURE ON CREEP-RUPTURE STRENGTH (9,10)

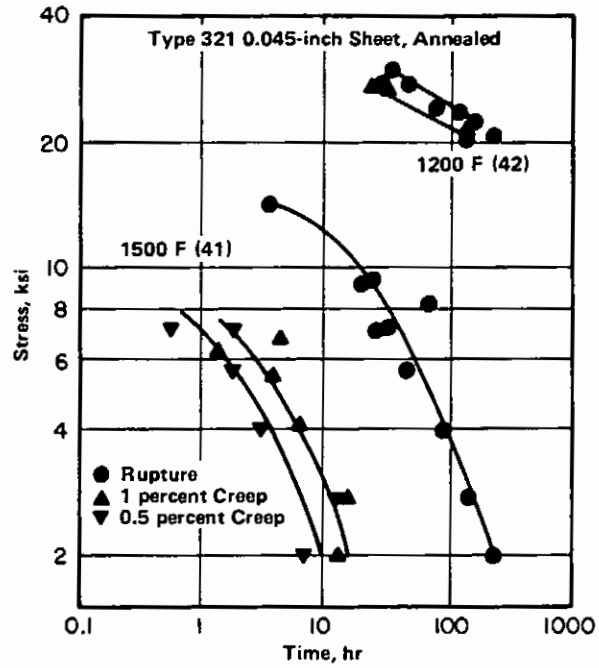

FIGURE 3.042. CREEP AND CREEP-RUPTURE CURVES FOR SHEET AT 1200 AND 1500 F (41,42)

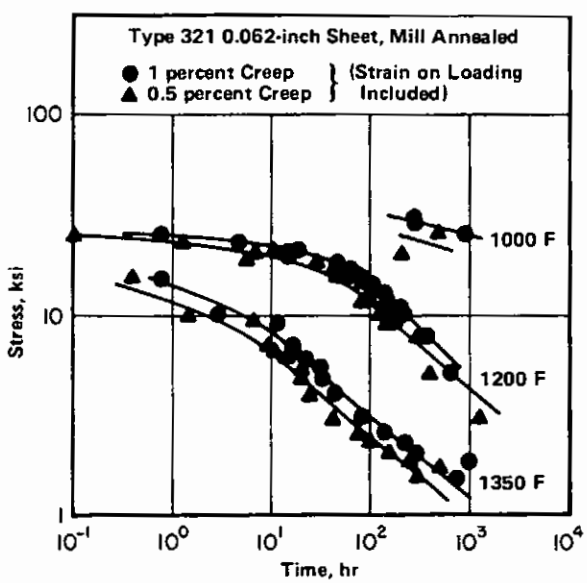

FIGURE 3.043. CREEP CURVES FOR SHEET AT 1000 TO 1350 F (72)

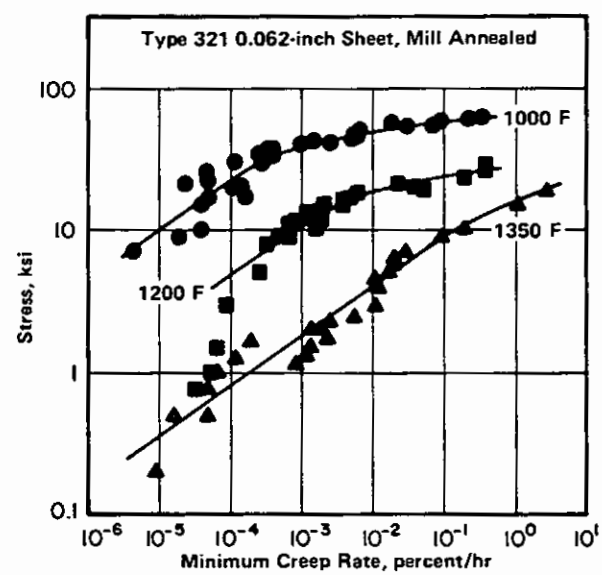

FIGURE 3.044. CREEP RATES FOR SHEET AT 1000 TO 1350 F (72)

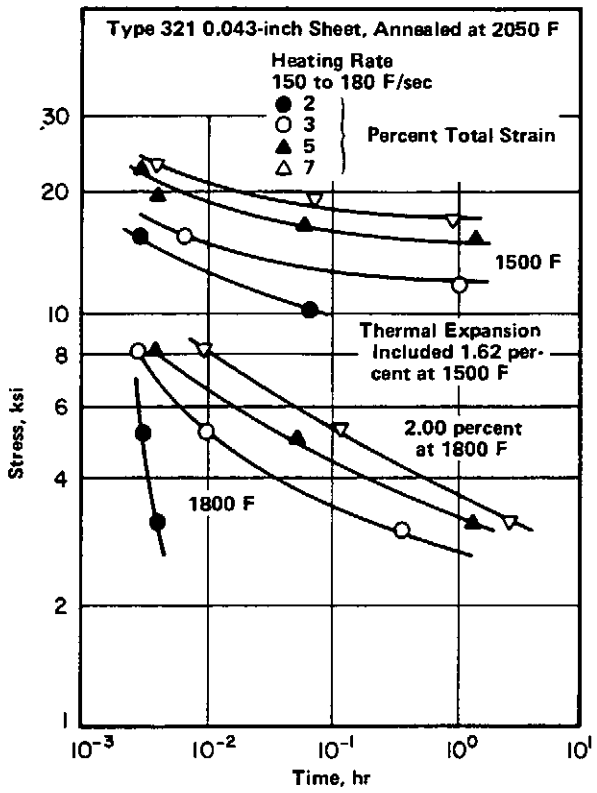

FIGURE 3.045. SHORT-TIME TOTAL-STRAIN CURVES FOR SHEET AT 1500 AND 1800 F (43)

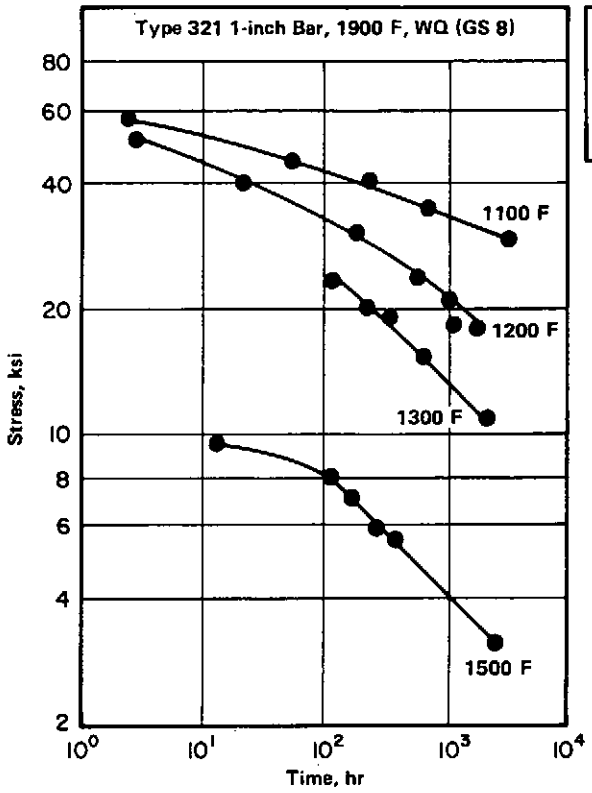

Fe
18 Cr
10 Ni
+ Ti

Type 321

FIGURE 3.046. CREEP-RUPTURE CURVES FOR BAR AT 1100 TO 1500 F (35)

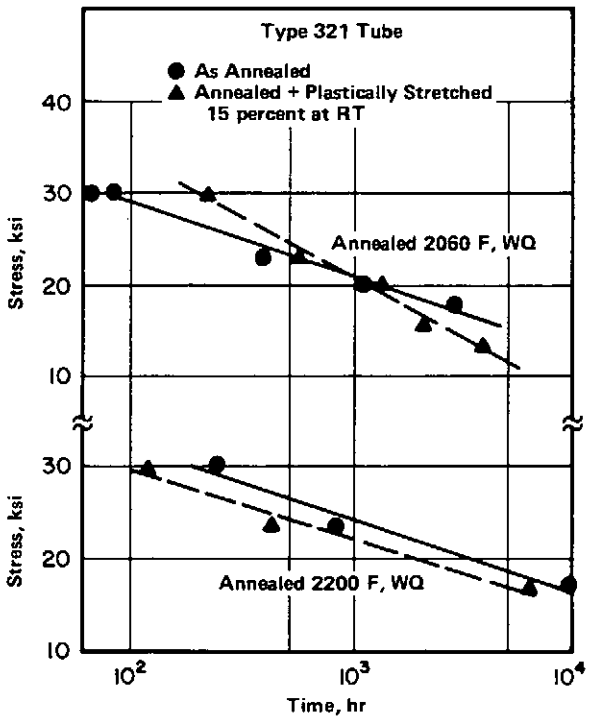

FIGURE 3.047. EFFECTS OF ANNEALING TEMPERATURE AND COLD WORK ON CREEP-RUPTURE PROPERTIES AT 1200 F (17)

Fe
18 Cr
10 Ni
+ Ti

Type 321

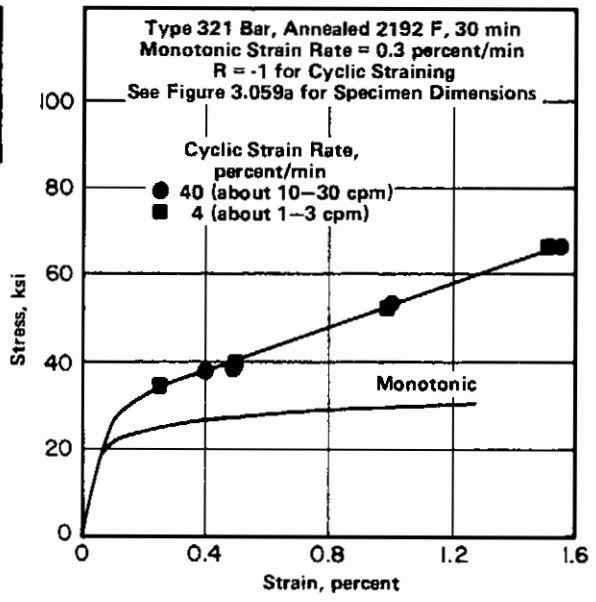

a. Room Temperature

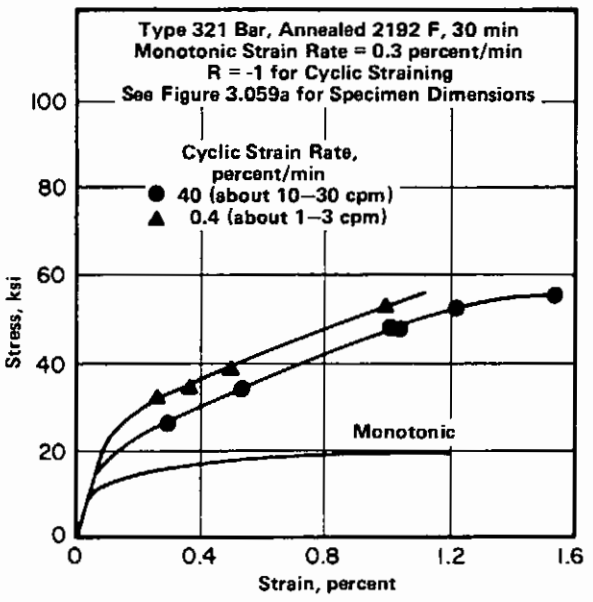

b. 842 F

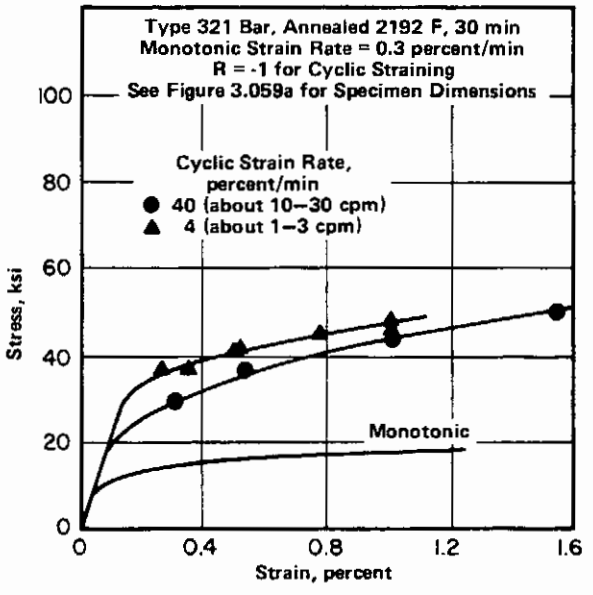

c. 1112 F

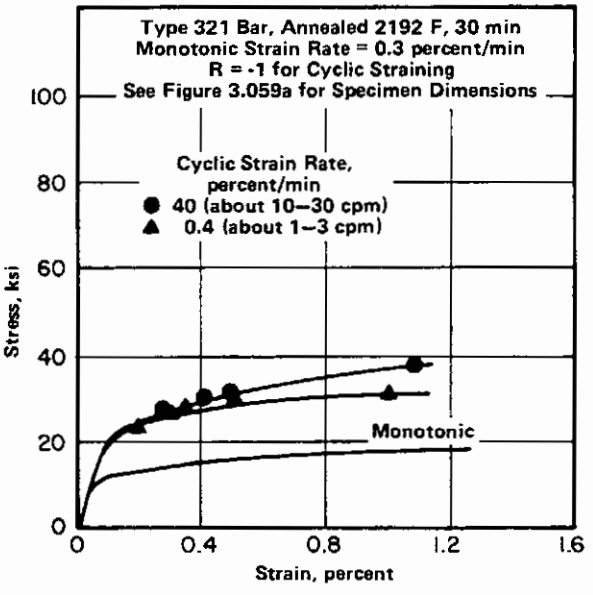

d. 1292 F

FIGURE 3.052. MONOTONIC AND CYCLIC STRESS-STRAIN CURVES FOR BAR AT ROOM AND ELEVATED TEMPERATURES (70)

Fe
18 Cr
10 Ni
+ Ti

Type 321

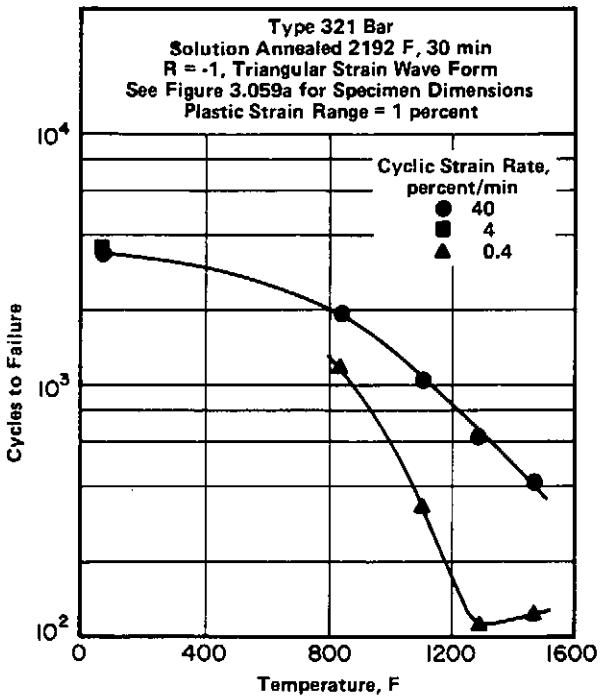

FIGURE 3.053. LOW-CYCLE FATIGUE LIFE AT ROOM AND ELEVATED TEMPERATURES (70,73)

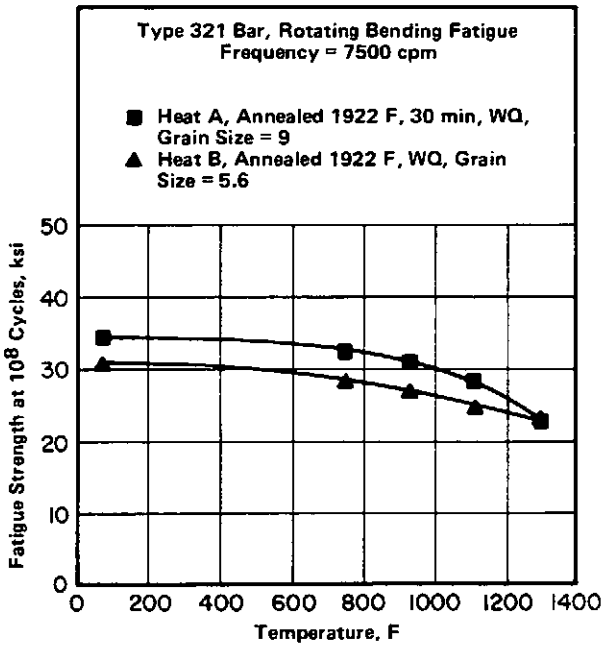

FIGURE 3.054. HIGH-CYCLE FATIGUE STRENGTH AT ROOM AND ELEVATED TEMPERATURES (73)

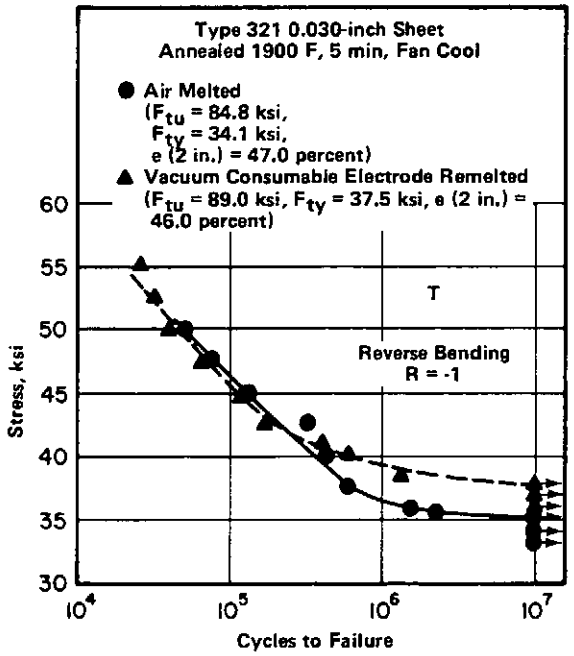

FIGURE 3.055. FATIGUE PROPERTIES OF AIR-MELTED AND VACUUM-MELTED SHEET (12)

Fe
18 Cr
10 Ni
+ Ti

Type 321

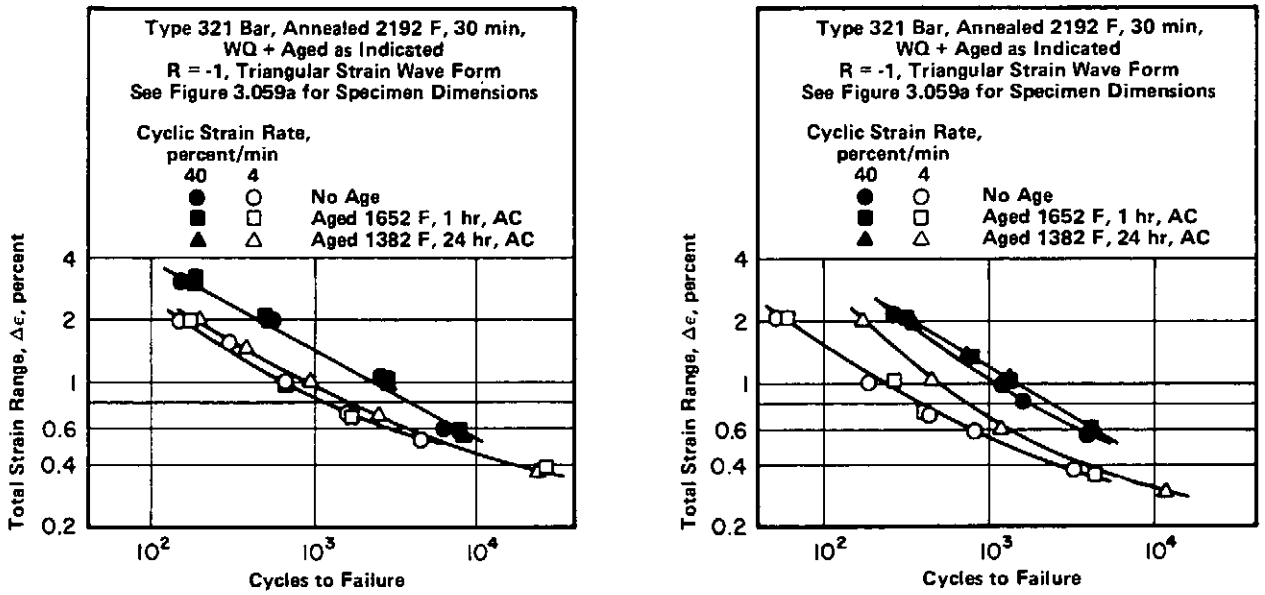

FIGURE 3.057. EFFECTS OF AGING AND CYCLIC STRAIN RATE ON FATIGUE BEHAVIOR AT ELEVATED TEMPERATURES (74)

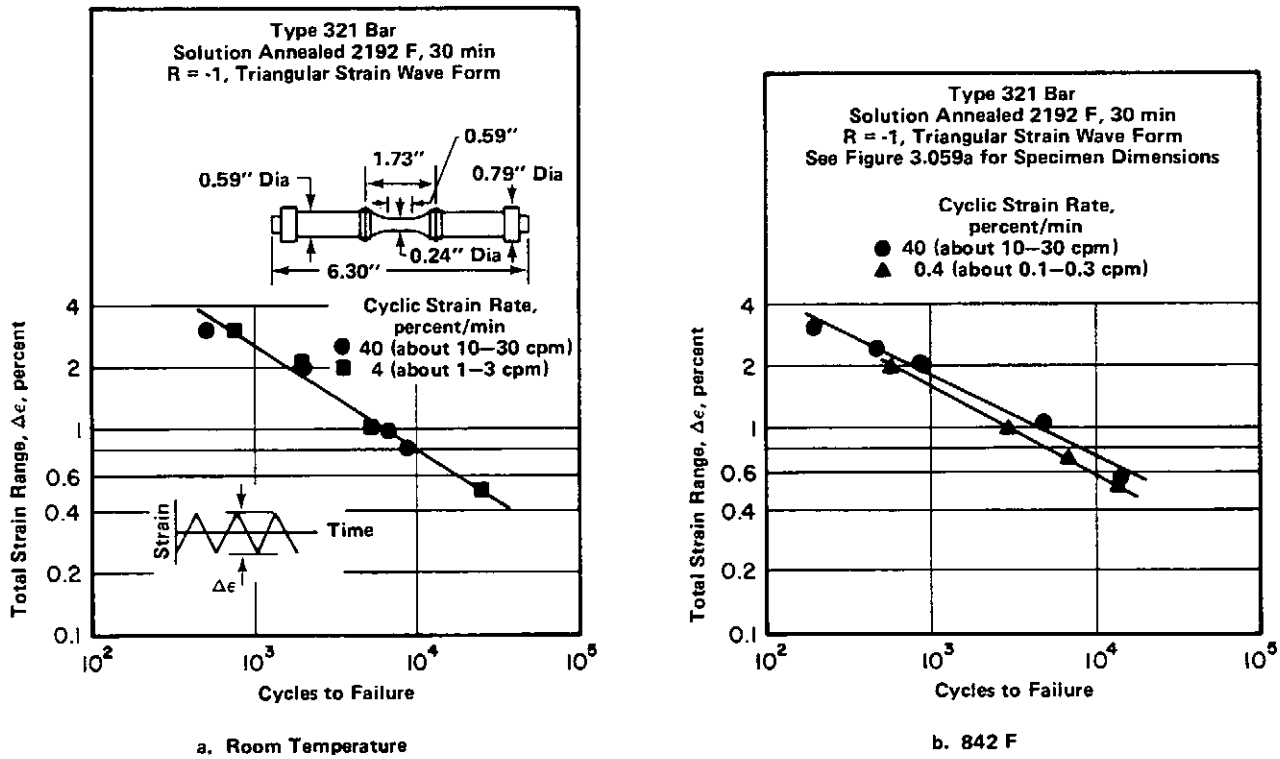

FIGURE 3.059. LOW-CYCLE AXIAL FATIGUE BEHAVIOR IN AIR AT ROOM AND ELEVATED TEMPERATURES (70, 73)

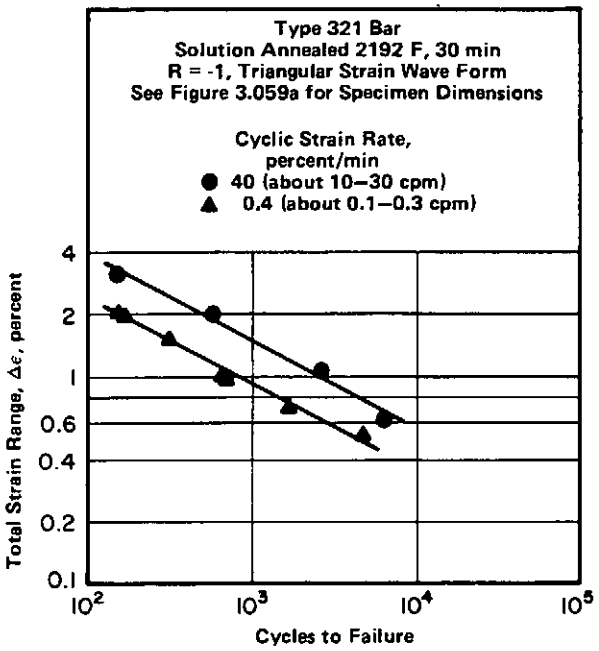

c. 1112 F

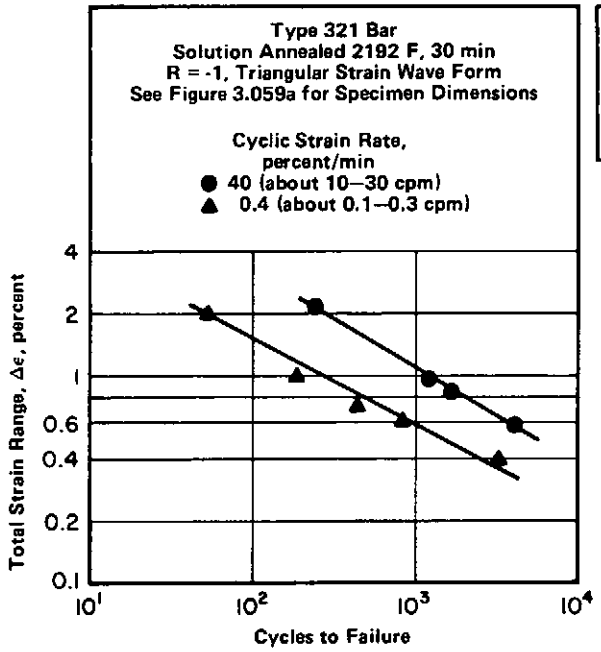

d. 1292 F

Fe
18 Cr
10 Ni
+ Ti

Type 321

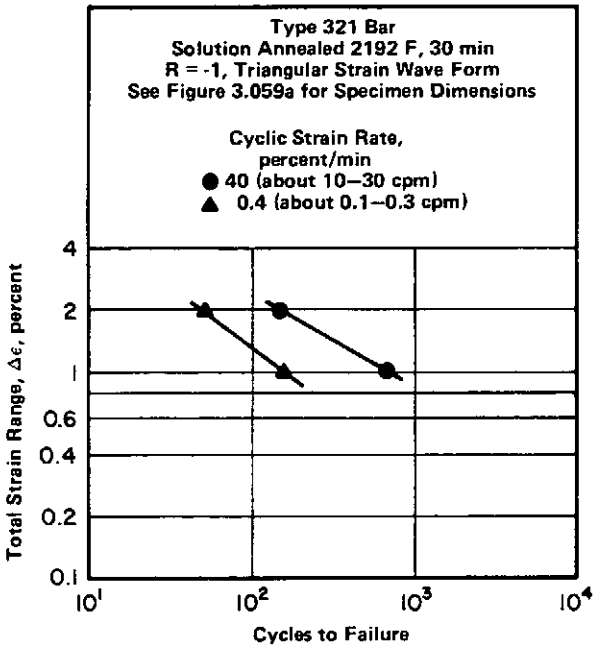

e. 1472 F

FIGURE 3.059. (CONTINUED)

Fe
18 Cr
10 Ni
+ Ti

Type 321

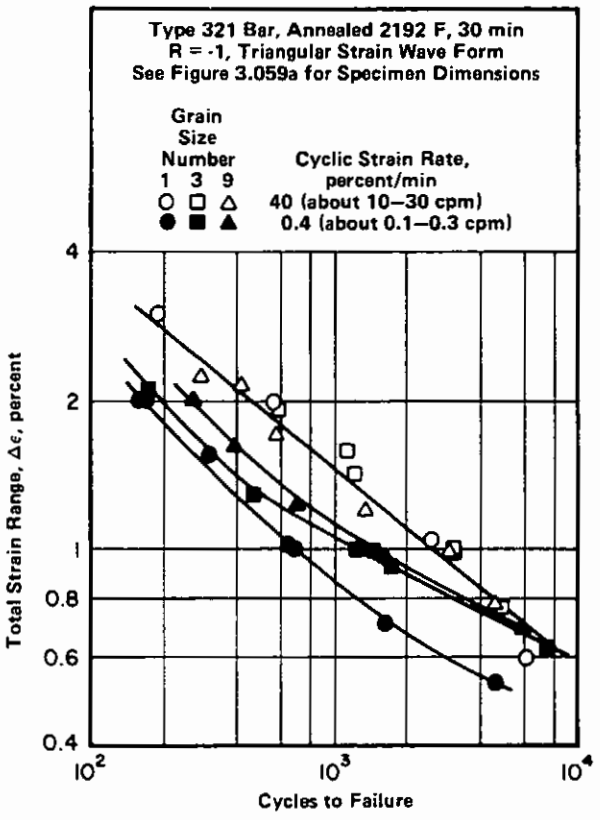

FIGURE 3.0511. EFFECTS OF GRAIN SIZE AND CYCLIC FREQUENCY ON AXIAL FATIGUE BEHAVIOR AT 1112 F (76)

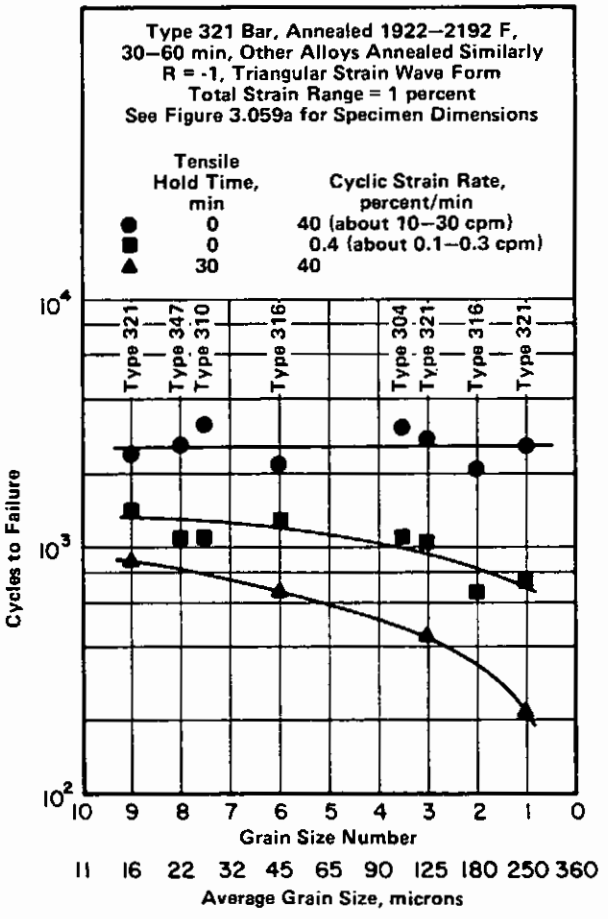

FIGURE 3.0512. EFFECTS OF GRAIN SIZE, CYCLIC FREQUENCY, AND HOLD TIME ON AXIAL FATIGUE LIFE OF AUSTENITIC STAINLESS STEELS AT 1112 F (76)

Fe
18 Cr
10 Ni
+ Ti

Type 321

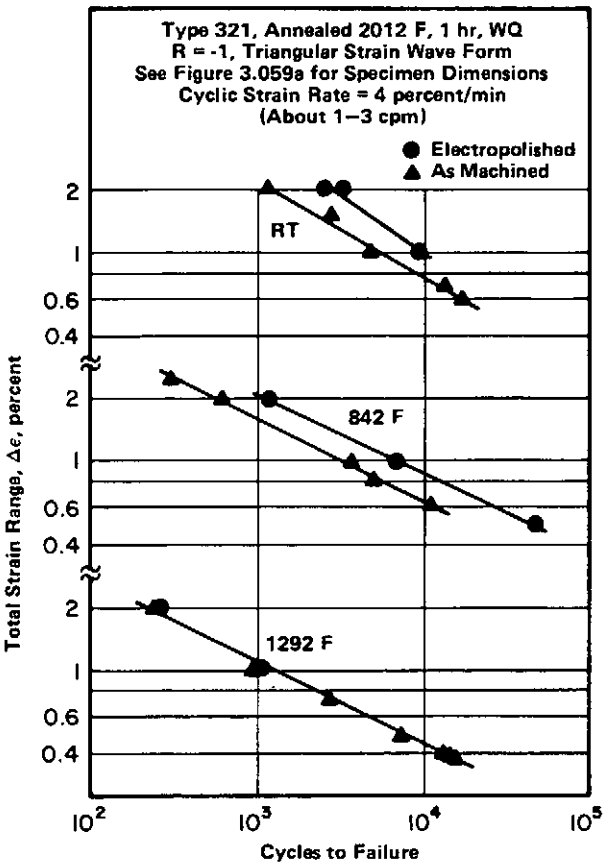

FIGURE 3.0514. EFFECT OF SURFACE FINISH ON AXIAL FATIGUE BEHAVIOR AT ROOM AND ELEVATED TEMPERATURES (75)

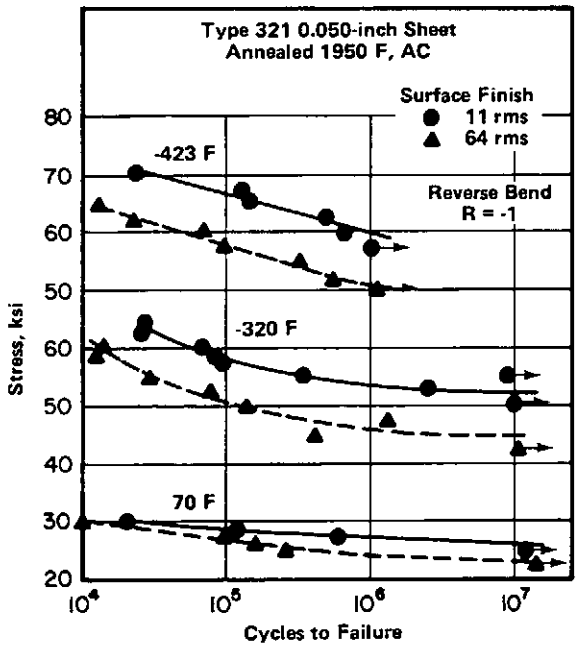

FIGURE 3.0515. EFFECTS OF LOW TEMPERATURES AND SURFACE FINISH ON FATIGUE PROPERTIES (13)

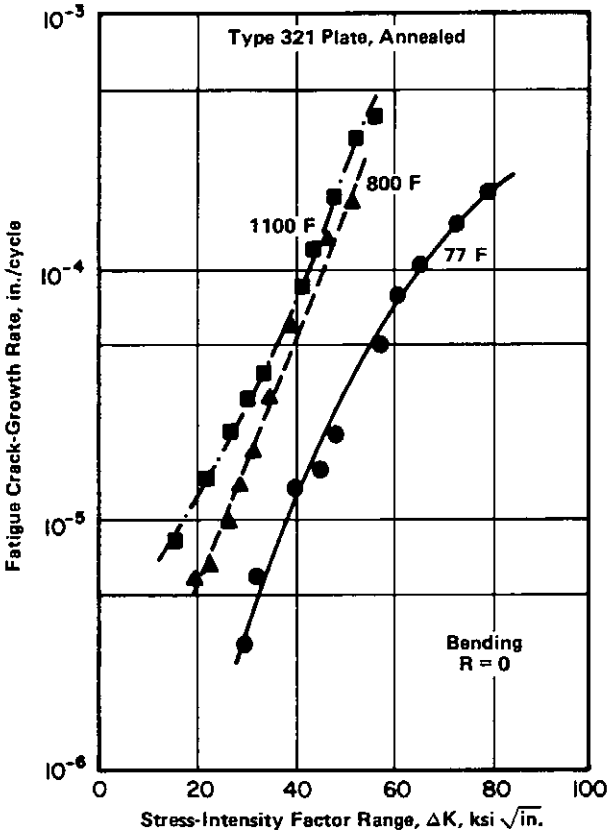

FIGURE 3.0516. FATIGUE CRACK-GROWTH RATE AS A FUNCTION OF THE STRESS-INTENSITY-FACTOR RANGE AT VARIOUS TEMPERATURES (22,32)

Fe
18 Cr
10 Ni
+ Ti

Type 321

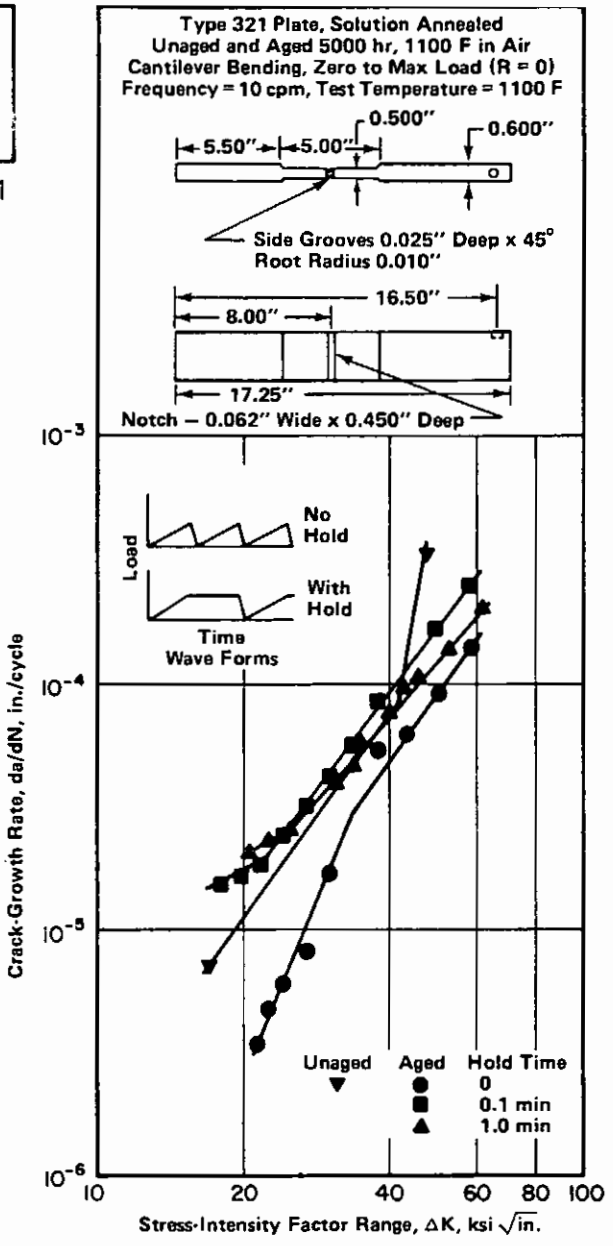

FIGURE 3.0518. EFFECTS OF AGING AND CYCLIC HOLD TIME ON BENDING-FATIGUE CRACK-GROWTH RATE AT 1100 F (77)

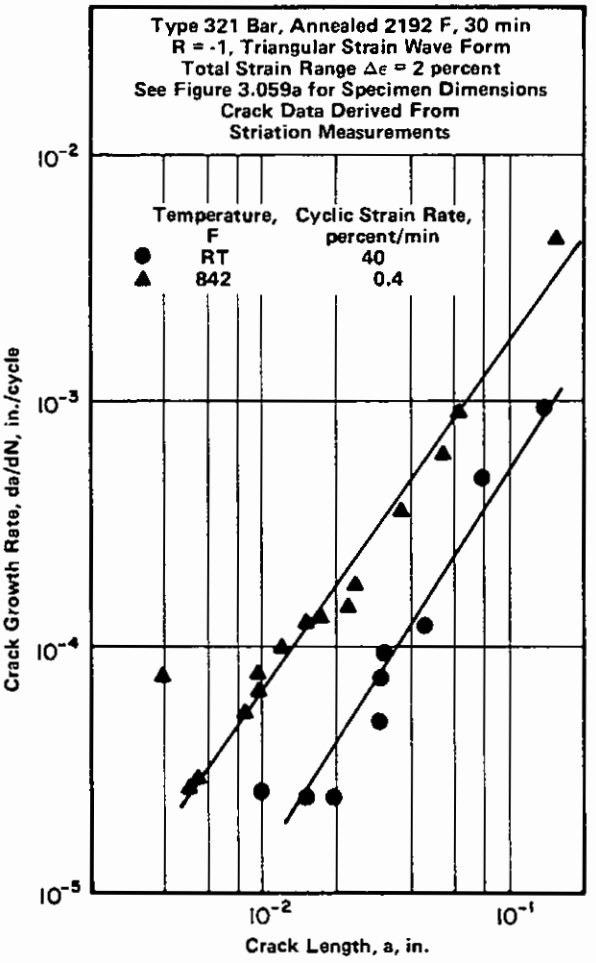

a. Room Temperature and 842 F

FIGURE 3.0520. RELATION BETWEEN CRACK-GROWTH RATE AND CRACK LENGTH AT ROOM AND ELEVATED TEMPERATURES (78)

Fe
18 Cr
10 Ni
+ Ti

Type 321

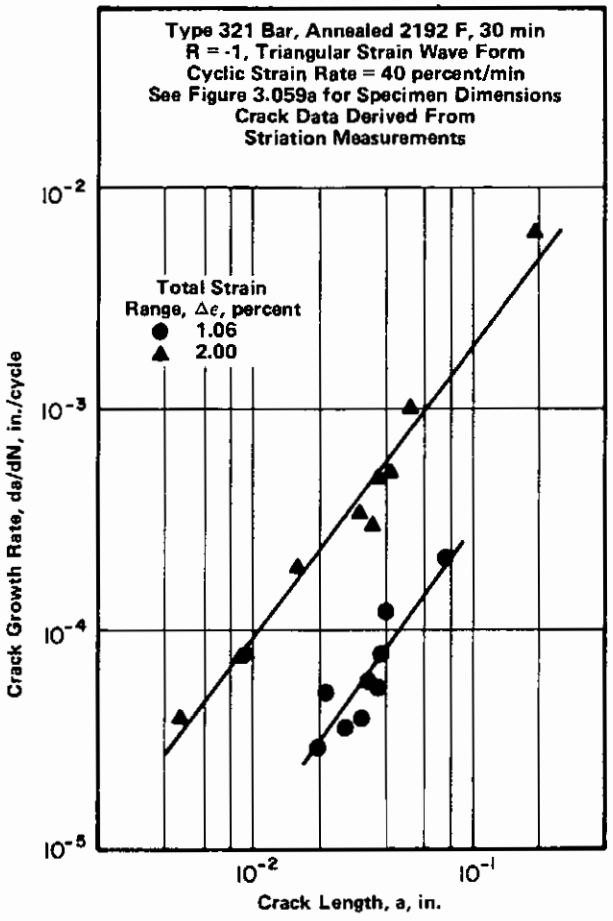

b. 1112 F

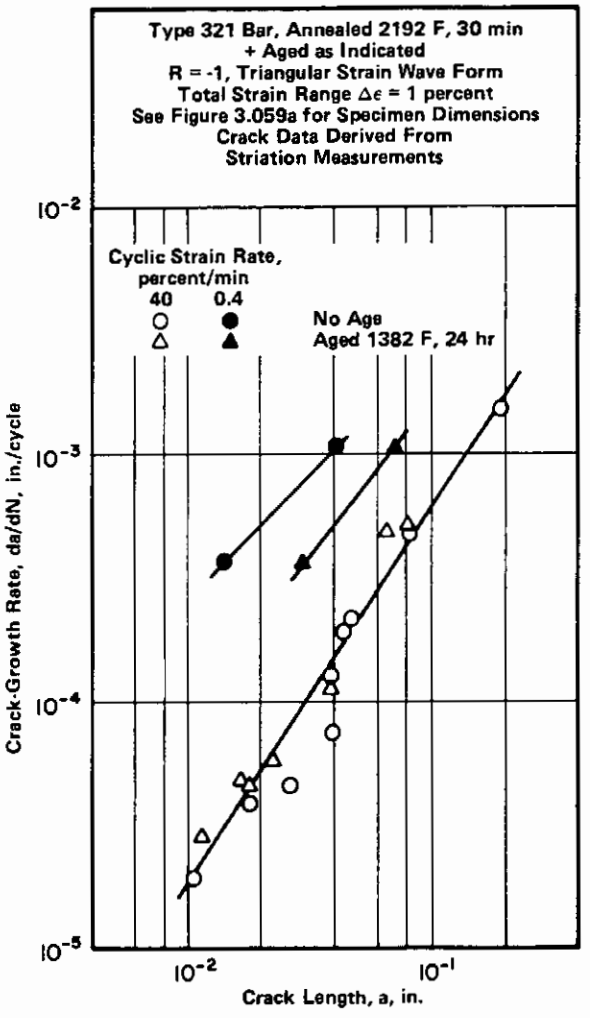

c. 1292 F

FIGURE 3.0520. (CONTINUED)

Fe
18 Cr
10 Ni
+ Ti

Type 321

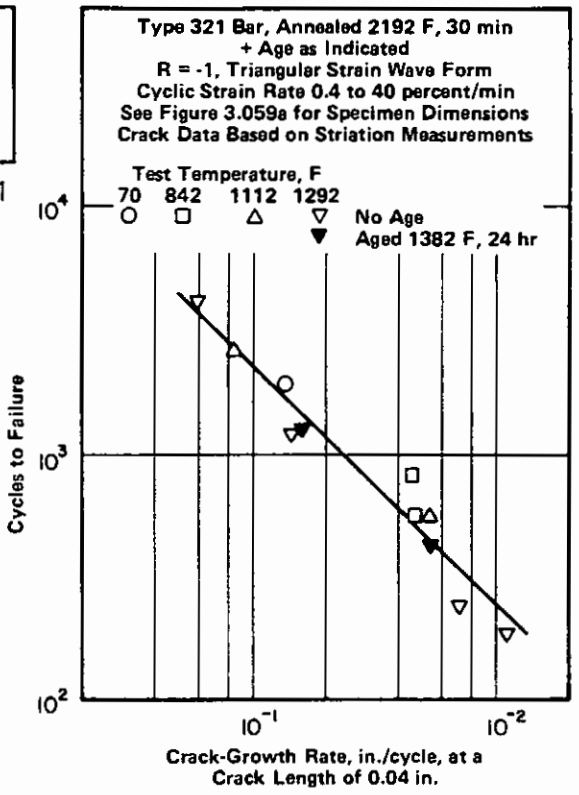

FIGURE 3.0521. RELATION BETWEEN FATIGUE LIFE AND CRACK-PROPAGATION RATE (78)

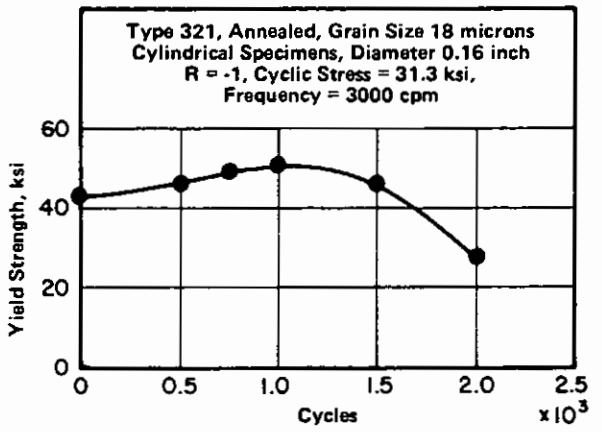

FIGURE 3.0523. EFFECT OF AXIAL FATIGUE ON SUBSEQUENT YIELD STRENGTH AT ROOM TEMPERATURE (71)

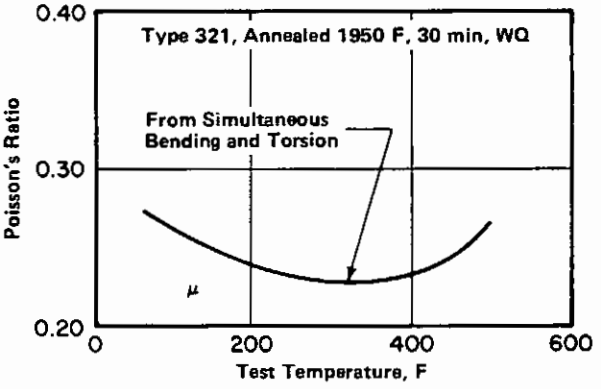

FIGURE 3.0611. EFFECT OF TEMPERATURE ON POISSON'S RATIO (38)

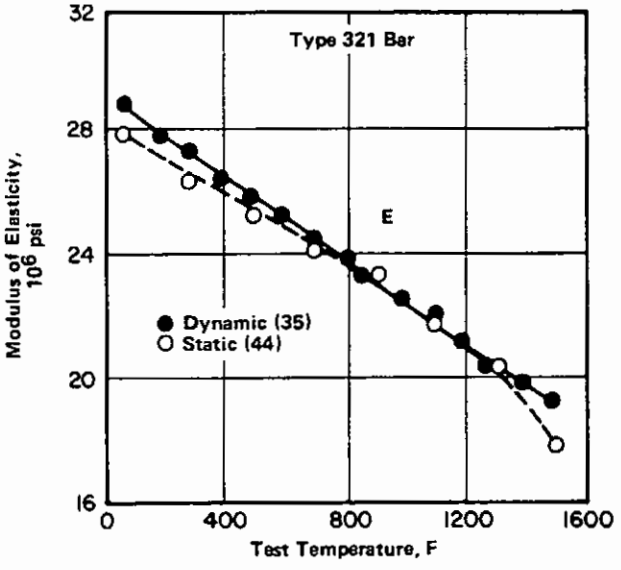

FIGURE 3.0621. MODULUS OF ELASTICITY AT ROOM AND ELEVATED TEMPERATURES (35,44)

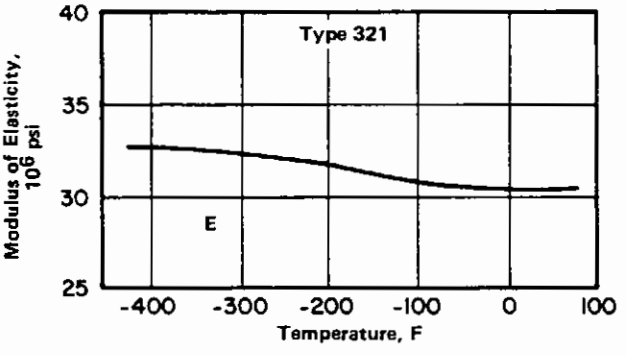

FIGURE 3.0622. MODULUS OF ELASTICITY AT LOW TEMPERATURES (38)

Fe
18 Cr
10 Ni
+ Ti

Type 321

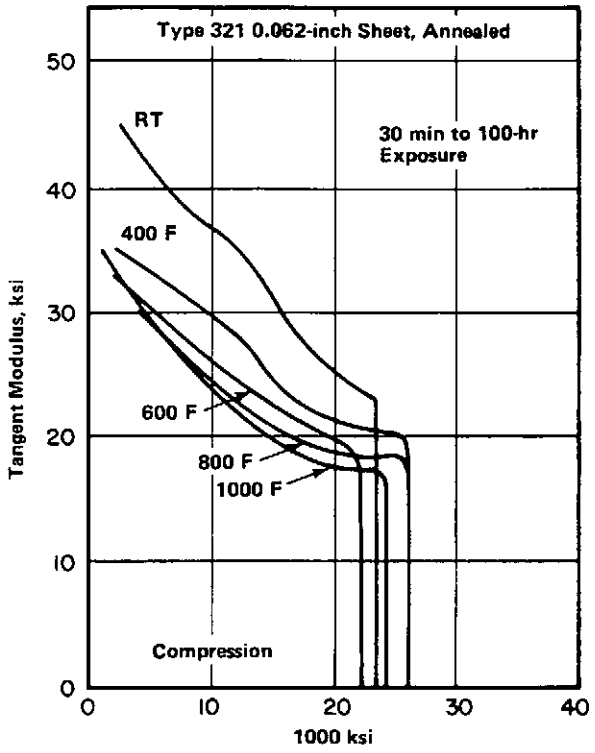

FIGURE 3.0623. TANGENT MODULUS CURVES IN COMPRESSION (36)

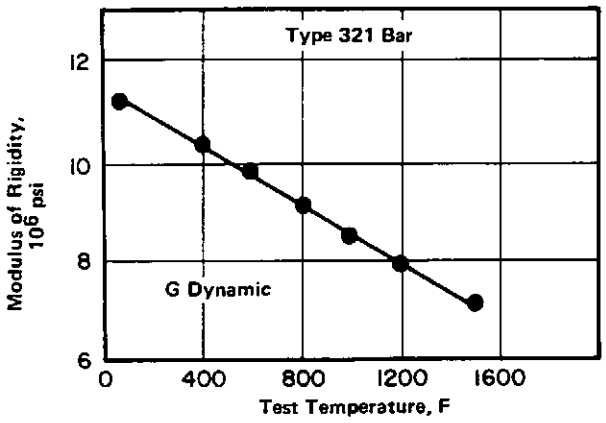

FIGURE 3.0631. MODULUS OF RIGIDITY AT ROOM AND ELEVATED TEMPERATURES (35)

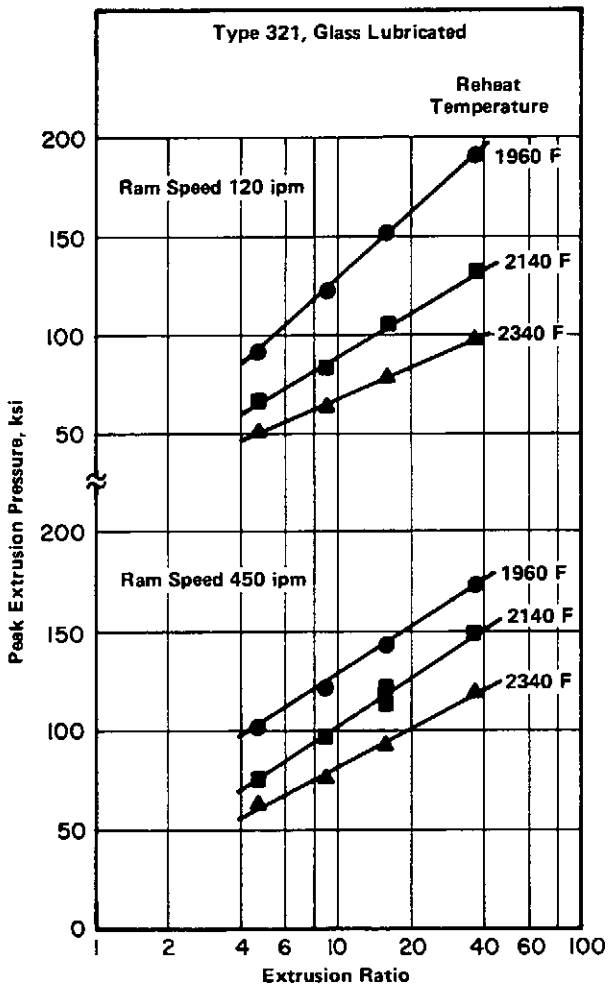

FIGURE 4.014. EFFECTS OF EXTRUSION RATIO, RE-HEAT TEMPERATURE, AND RAM SPEED ON PEAK EXTRUSION PRESSURE (79)

Fe
18 Cr
10 Ni
+ Ti

Type 321

Alloy	Type 321			
Form	Sheet and Plate			
Condition	Annealed			
Material Thickness, in.	Type Weld	F_{ty}, ksi	F_{tu}, ksi	e (2 in.), percent
0.060	Parent Metal	40.1	92.1	48.8
	Low Voltage	39.6	92.7	55.6
	High Voltage	39.4	91.7	44.0
0.125	Parent Metal	42.7	89.3	48.6
	Low Voltage	43.7	89.0	39.0
	High Voltage	43.6	88.0	33.3
0.800	Parent Metal	28.9	79.3	66.3
	Low Voltage	31.8	80.0	60.3
	High Voltage	30.7	82.3	62.0

TABLE 4.0311. TENSILE PROPERTIES OF SPECIMENS BUTT-WELDED IN VACUUM BY LOW-VOLTAGE ELECTRON-BEAM PROCESSES; NO PREHEAT OR POSTHEAT TREATMENTS (20)

Alloy	Type 321	
Condition	Annealed	
Form	Brazed Joints	
Braze Temp, F	1800	1850
F_{su}, ksi	68.0	77.3

Note: Brazed in vacuum with 82 percent gold – 18 percent nickel brazing alloy.

TABLE 4.0321. SHEAR STRENGTH OF BRAZED JOINTS (18)

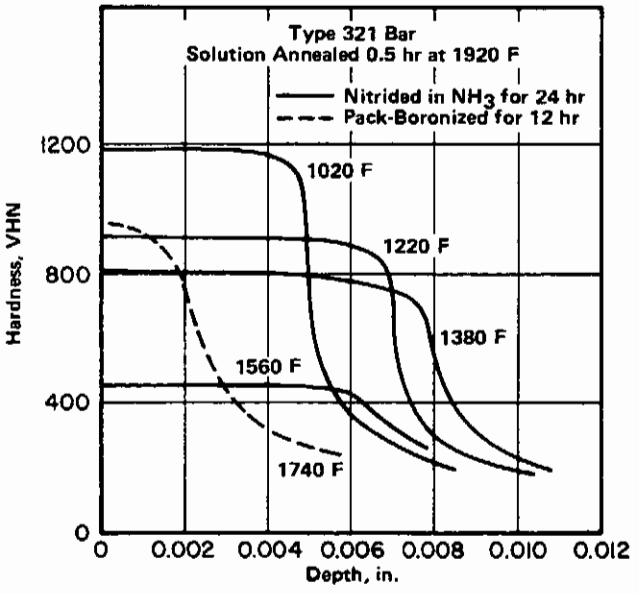

FIGURE 4.045. HARDNESS-DEPTH PROFILES FOR TYPE 321 AFTER NITRIDING AT 1020 TO 1560 F OR BORONIZING AT 1740 F (82,83)